Final Report

Project Title: Low Cost High Performance Nanostructured Spectrally Selective Coating

Project Period: 8/1/12 – 3/31/15

Budget Period: Phase 3, 4/1/14 - 3/31/15

Project Budget: $125,000 ($100,000 DOE, $25,000 cost share)

Submission Date: 05/16/15

Recipient: University of California, San Diego

Address: 9500 Gilman Dr.

          La Jolla, CA 92093

Award Number: DE- EE0005802

Project Team: University of California, San Diego

Contacts: Sungho Jin
          Distinguished Professor and Iwama Endowed Professor of
          Materials Science
          University of California, San Diego
          Phone: 858-534–4903
          Email: jin@ucsd.edu

Executive Summary

Solar absorbing coating is a key enabling technology to achieve high-temperature high-efficiency concentrating solar power operation. A high-performance solar absorbing material must simultaneously meet all the following three stringent requirements: high thermal efficiency (usually measured by figure of merit), high-temperature durability, and oxidation resistance. The objective of this research is to employ a highly scalable process to fabricate and coat black oxide nanoparticles onto solar absorber surface to achieve ultra-high thermal efficiency. Black oxide nanoparticles have been synthesized using a facile hydrothermal process and coated onto absorber metal surface. The material composition, size distribution and morphology of the nanoparticle are guided by numeric modeling. Optical and thermal properties, such as solar and infrared absorptance and reflectance have been both modeled and measured. High temperature durability has been achieved by using nanocomposites and high temperature annealing. Mechanical durability on thermal cycling have also been investigated and optimized. The research outcomes demonstrate that **all the project milestones have been achieved** with the innovative solar absorbing coating developed at UCSD. Therefore, this technology is promising for commercial applications in next-generation high-temperature concentration solar power (CSP) plants

Table of Contents

1   Background

Future improved parabolic trough and tower CSP devices are expected to operate at 750 ^{o}C or above, meaning the spectral selective coating (SSC) on solar absorbers will have to be stable, i.e., do not get oxidized at ~750 ^{o}C . It is desirable that the SSC maintains its structural integrity and optical properties during its entire lifetime (over 20-30 years).

In the case of parabolic trough systems, while some solar absorbers are continuously operated in vacuum (~10^{-5} torr) to prevent convective and conductive heat loss, SSCs could still be exposed to air for a short time in case of vacuum failures or during shipping and storage. Sunlight receiver failures lead to costly O&M expenses.

On the other hand, for solar towers, it is expected that the solar absorbers will be operated in ambient, thereby suggesting the need for high temperature durability and oxidation resistance in addition to high thermal absorbing efficiency.

2   Introduction

The overall objective of the project is to develop solar absorbing materials with high solar absorption (and hence high thermal efficiency) that also exhibits superb high-temperature durability and excellent oxidation resistance, desirably at a high temperature of ~750 ^{o}C for improved efficiency operation of the future CSP technology as identified in the roadmap of the DOE Sunshot program.

Our work in the Budget Period 2 specifically focuses on the study of high temperature oxidation resistant coating materials for high-temperature SSC. Various ongoing target materials as well as some new materials have been synthesized, optical properties measured and high temperature thermal, optical and mechanical behavior evaluated.

In this report, we will first describe the research methodology and technical approaches employed in this project (section 3), which are primarily divided into three distinctive and yet coupled components:

1. **Synthesis of black oxide materials**
2. **Preparation of solar absorbing coatings**
3. **Optical and thermal characterization of the coatings**

Subsequently, we will present and discuss the key research findings (section 4), in accordance with the targets outlined in the statement of project objectives (SOPO).

Finally, we will draw conclusions based on the findings and also point out future outlook of the technology.

3 Technical Approaches

3.1 Overview of technical approaches

We have formed a multi-disciplinary team to tackle the multi-faceted problem of developing the high performance solar absorbing materials. **Fig. 1** shows the overview of research activities and technical approaches employed throughout this work.
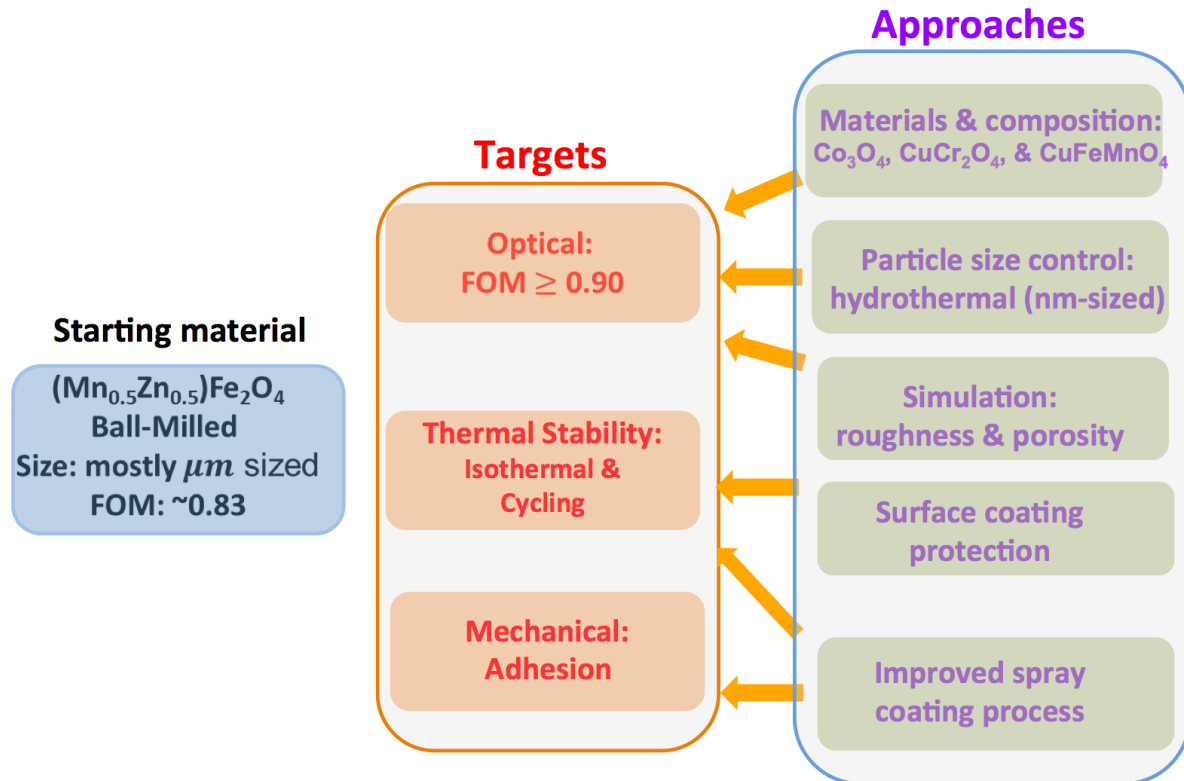
Fig. 1. Overview of research activities and technical approaches employed throughout this work. The developed SSC layers are expected to possess a combination of high performance merits, including high optical performance, measured by a figure of merit (FOM) greater than 0.90, excellent thermal durability and oxidation resistance, and excellent adhesion to the underlying substrates. To simultaneously meet these demanding and multi-facet requirements, multi-disciplinary approaches are pursued, including materials synthesis, optimization and processing, nanostructuring, optical and thermal measurements and modeling.

3.2 Development of Optimal Black Oxide Materials for Solar Absorbers

To accelerate the R&D efforts, we have investigated, in parallel, several different black oxide materials, namely, Mn-Zn ferrites, Co ferrites, and Co oxides (Co_3O_4), Cu chromite (CuCr2O4), and CuFeMnO4. We have identified there most promising materials and their combinations, namely, **Co3O4, CuCr2O4, and CuFeMnO4**. Our best coating material can simultaneously meet all the stringent requirements needed for high-performance solar absorbing, which is significantly superior to the state of the art commercial material, namely, Pyromark®.

In our previous reports, we have described in detail the synthesis of Mn-Zn ferrites and Co ferrites. Here we will focus on the reporting the synthesis of the three important oxides we have developed within this project, namely, **Co_3O_4, $CuCr_2O_4$, and $CuFeMnO_4$,** as these oxide materials exhibit the best performance.

3.2.1 Cobalt Oxide (Co_3O_4) Nanoparticles and Nanorods

Cobalt oxide (Co_3O_4) has a relatively low bandgap energy which is 0.47 eV (2.64 µm, at the temperature of 250K) so that the high solar absorption effect is expected. Cobalt oxide NPs were made by the hydrothermal synthesis, which is similar to the previous MnZn-ferrites method. Specifically, cobalt chloride salt was used as a precursor material and the temperature of hydrothermal synthesis was 150 ^{o}C for 20 hours. The synthesized Co_3O_4 NPs and annealed NPs were observed with SEM as shown in **Fig. 2 (a) and (b),** respectively.

In order to increase the crystallization and the thermal stability, the synthesized cobalt oxide particles were annealed at 750°C for 2 hr in air after which particle size increased to 100-300 nm and the color was black. By means of EDX composition analysis, the annealed particles proved to be cobalt oxide as shown in **Fig. 2(c)**.

| Element	Weight%	Atomic%
O K	26.87	57.51
Co L	73.13	42.49
Totals	100.00	
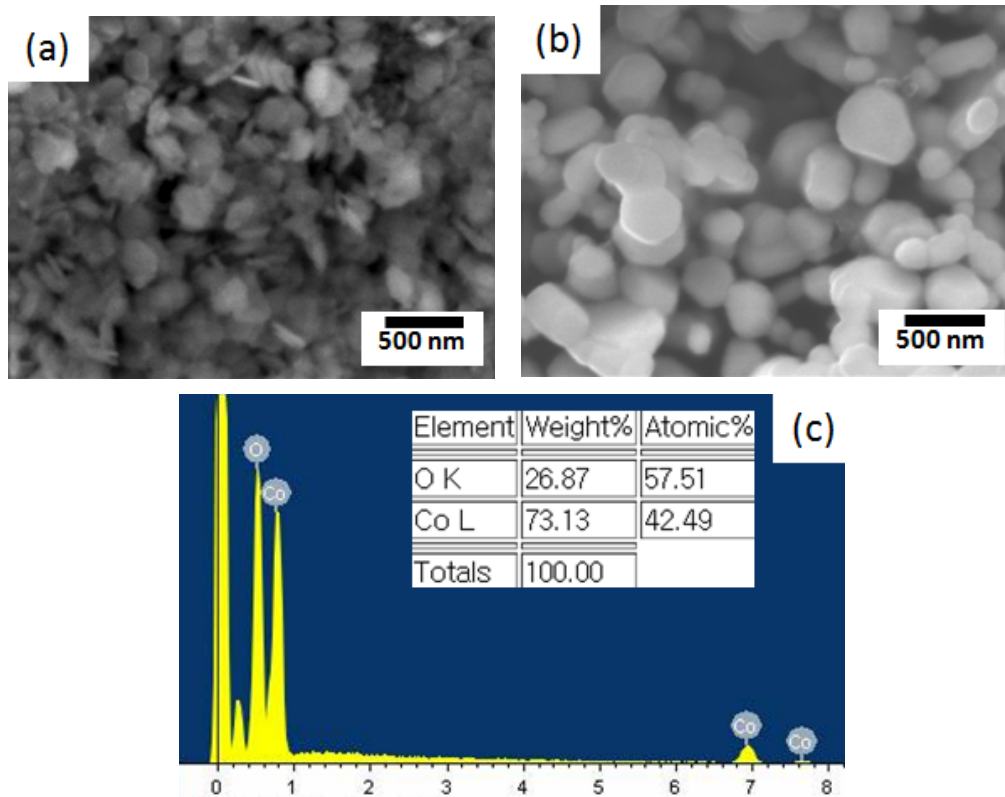
Fig.2. SEM images showing cobalt oxide nanoparticles (a) as-synthesized and (b) after annealing at 750 ^{o}C for 2 hr, and (c) EDX analysis results.

The X-ray diffraction pattern of Co oxide powders after stabilizing at 750°C for 2 hoursi shown in **Fig. 3**, confirming the Co_3O_4 phase
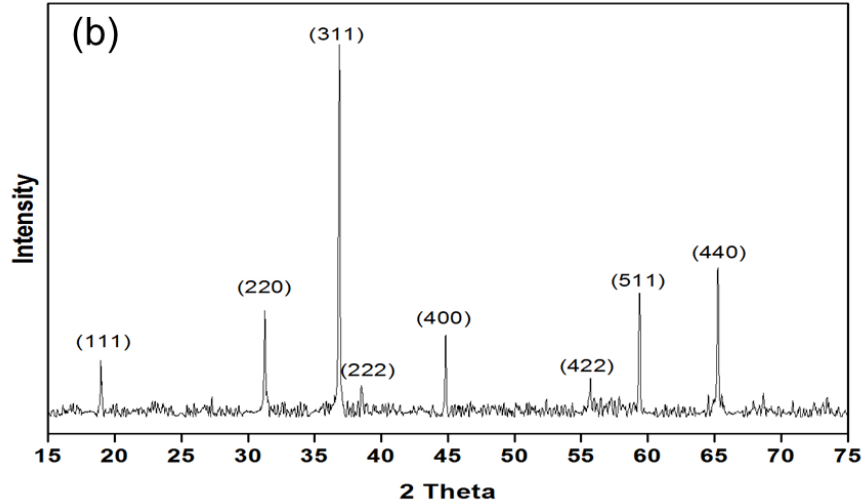
Fig. 3. X-ray diffraction pattern of Co oxide powders after stabilizing at 750°C for 2 hours, showing the Co_3O_4 phase.

Secondly, nanorods of cobalt oxide was synthesized by hydrothermal method using cobalt chloride salt and urea ($CO(NH_2)_2$) at 105 ^{o}C for 10 hr. After drying precipitates in a vacuum oven, the annealing process was made at 300 ^{o}C for 3 hr in air. Based on the previously published research [3] on cobalt oxide made by this method was found to be Co_3O_4 which has a bandgap of 1.28 eV (0.969 μm). The synthesized nanorods of Co_3O_4 has black color, which is caused by the bandgap as low as Co-ferrite. The images and size information are summarized in **Fig. 4** and **Table 1**. As seen in **Fig. 4**(c), obtained was EDX analysis result, which shows that Co ratio of nanorods is smaller than that of cobalt oxide particles. Therefore, cobalt oxide particles can be estimated to be Co_3O_4 by EDX comparison between particles and nanorods and cobalt oxide nanorods are expected to be Co_3O_4 based on the published research data [3]. Two types of cobalt oxide nanorods were formed including long rods with high aspect ratio and short rods with low aspect ratio as summarized in Table 1. These various cobalt oxide nanorods can be highly expected to increase the solar absorption when applied for CSP light receiver materials.

Element	Weight%	Atomic%
O K	31.78	63.18
Co L	68.22	36.82
Totals	100.00	
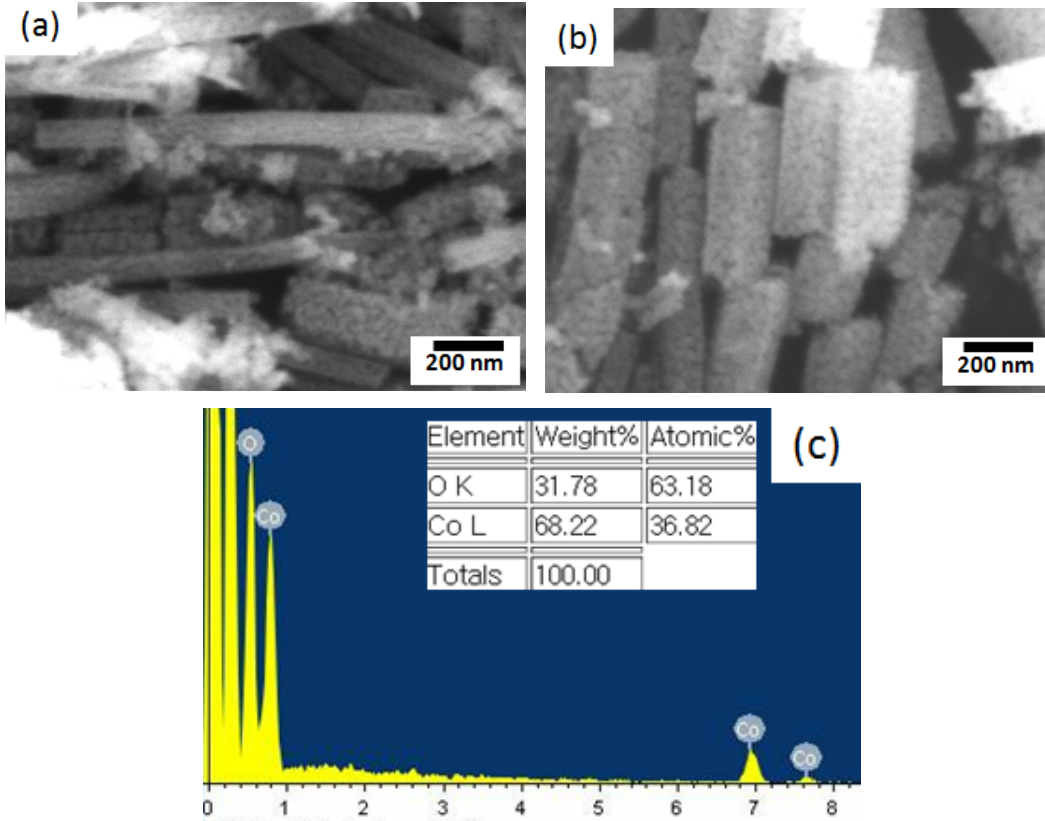
Fig.4. SEM images showing cobalt oxide (Co_3O_4) nanorods ; (a) long nanorods with high aspect ratio and (b) short nanorods with low aspect ratio. And (c) EDX analysis result.

Table 1. The synthesis condition and properties of cobalt oxide particles

	Synthesis Condition	Size	Color
Cobalt oxide Particles	Hydrothermal : pH < 11, 150 ^{o}C, 20 hr	As-synthesized 50-300 nm → Annealed 100-300nm	Black (Annealed)
Cobalt oxide Nanorods	Hydrothermal : 105 ^{o}C, 10 hr → Anneal : 300 ^{o}C, 3 hr, Air	Annealed at 300 ^{o}C Long rod : L 1μm, D 100 nm Short rod : L 200-500 nm, D 150 nm	Black

3.2.2 Cu Chromite nanoparticles

Copper chromite can have two types of atomic compositions including $Cu_2Cr_2O_5$ or $CuCr_2O_4$. The composition has to be optimized to obtain a higher FOM value. Copper chromite nanoparticles were synthesized with different atomic ratio (Cu/Cr=1/1, and 1/2) and crystallized at 550 ^{o}C /5h/air and 750 ^{o}C /2h/air as a final synthesis step. As shown in **Fig. 5**, the particles crystallized at 550 ^{o}C/5h/air have smaller size (< 50 nm) than those crystallized at 750 ^{o}C/2h/air (200 nm - 1μm).
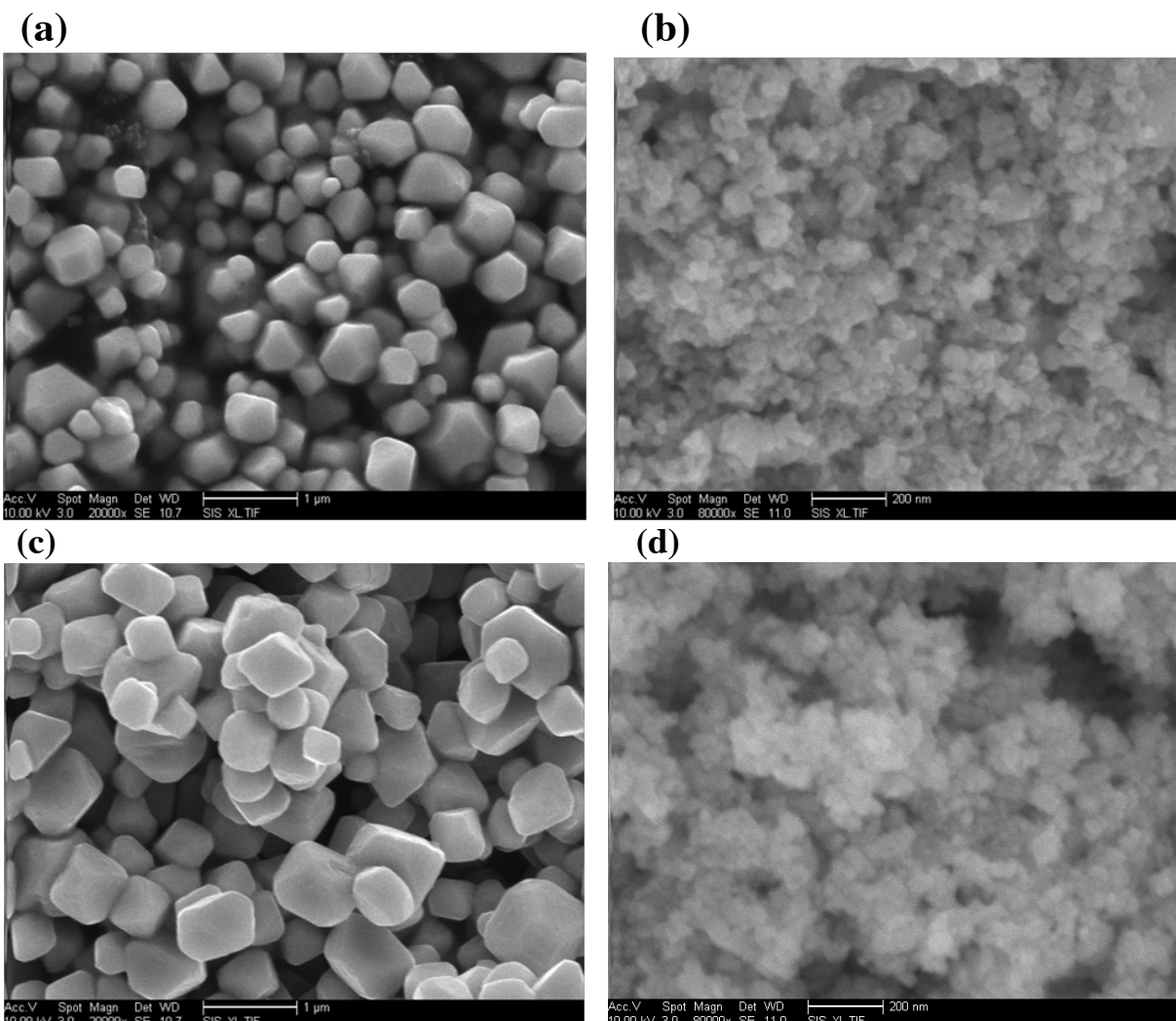
Fig. 5. Copper chromite particles synthesized with conditions of (a) Cu/Cr = 1/1 and crystallization at 750 ^{o}C/2h/air, (b) Cu/Cr = 1/1 and crystallization at 550 ^{o}C/5h/air, (c) Cu/Cr = 1/2 and crystallization at 750 ^{o}C/2h/air, and (d) Cu/Cr = 1/2 and crystallization at 550 ^{o}C/5h/air. Scale bar: 1 μm for (a) and (c), and 200 nm for (b) and (d).

The reflectance data in **Fig.6** shows that the SSC layers made of copper chromite particles with atomic ratio of Cu/Cr=1/2 and crystallized at 550 ^{o}C/5h/air have the best FOM value (0.8919) among the four samples. The preferred composition of copper chromite and crystallization temperature is therefore decided to be $CuCr_2O_4$ and 550 ^{o}C /5h/air.
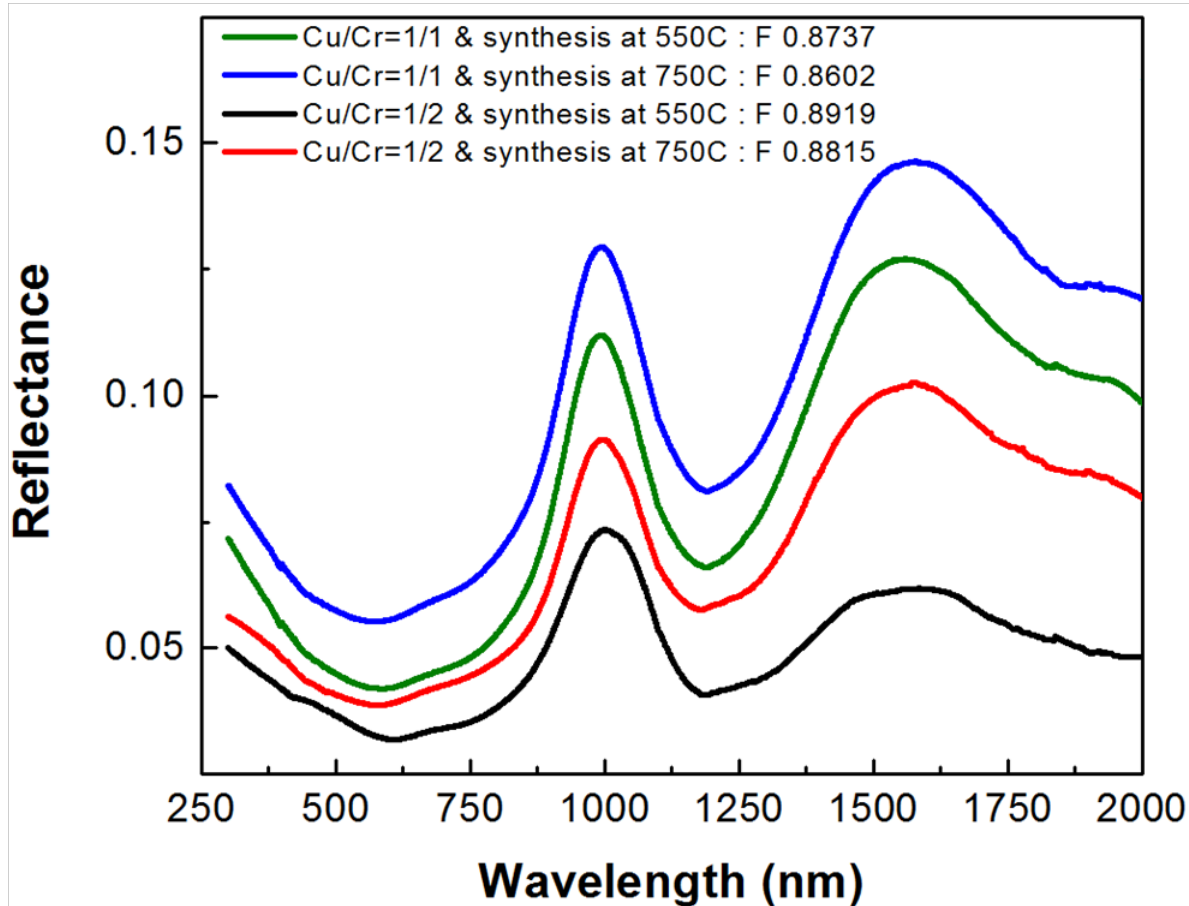
Fig.6. Reflectance change of SSC layers made of copper chromite nanoparticles with different atomic ratio (Cu/Cr) and crystallized at different temperatures. All coated samples were annealed with conditions of 750 ^{o}C/2h/air before reflectance measurement.

3.2.3 Copper Iron Manganese Oxide (CuFeMnO$_4$) Nanoparticles

The third black oxide, copper iron manganese oxide, was synthesized hydrothermally with different atomic compositions: Cu/Fe/Mn = 1/1/1, 0.5/0.5/2.0, 1.125/0.75/1.125, 2.0/0.5/0.5, and 0.5/2.0/0.5. **Fig. 7** shows the CuFeMnO$_4$ particles synthesized with the atomic ratio of Cu/Fe/Mn=1/1/1 and crystallized at 550 ^{o}C/5h/air. The particle size ranges from 100 nm to 300 nm.

SSC layers were fabricated with copper iron manganese oxide particles having various atomic compositions aforementioned without using pore-forming polymer beads and their reflectance was measured after annealing at 750 ^{o}C/2h/air. Based on the reflectance data shown in **Fig. 8**, a larger amount of Fe results in higher reflectance and a lower FOM (eg. Cu/Fe/Mn=0.5/2.0/0.5, FOM=0.8547). Also, a larger amount of Cu leads to higher reflectance and a lower FOM (eg. Cu/Fe/Mn=2.0/0.5/0.5, FOM=0.8654). Among the five samples with different compositions we studied here, the SSC layer made of particles with the ratio of Cu/Fe/Mn=1/1/1 exhibits the lowest reflectance and best FOM value (0.8809).
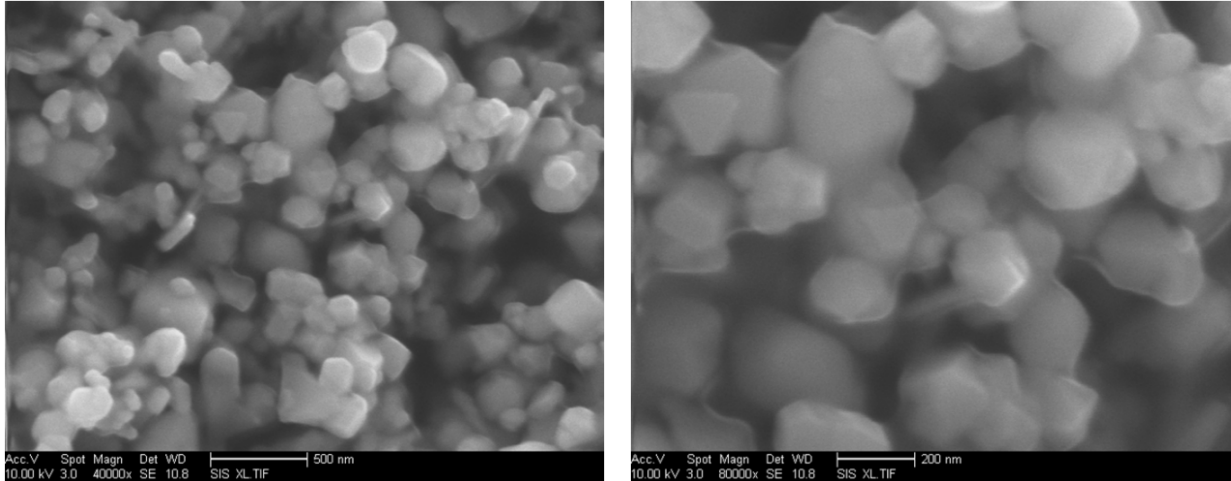
Fig. 7. Copper iron manganese (CuFeMnO$_4$) particles observed with SEM have particle size of 100-300 nm.
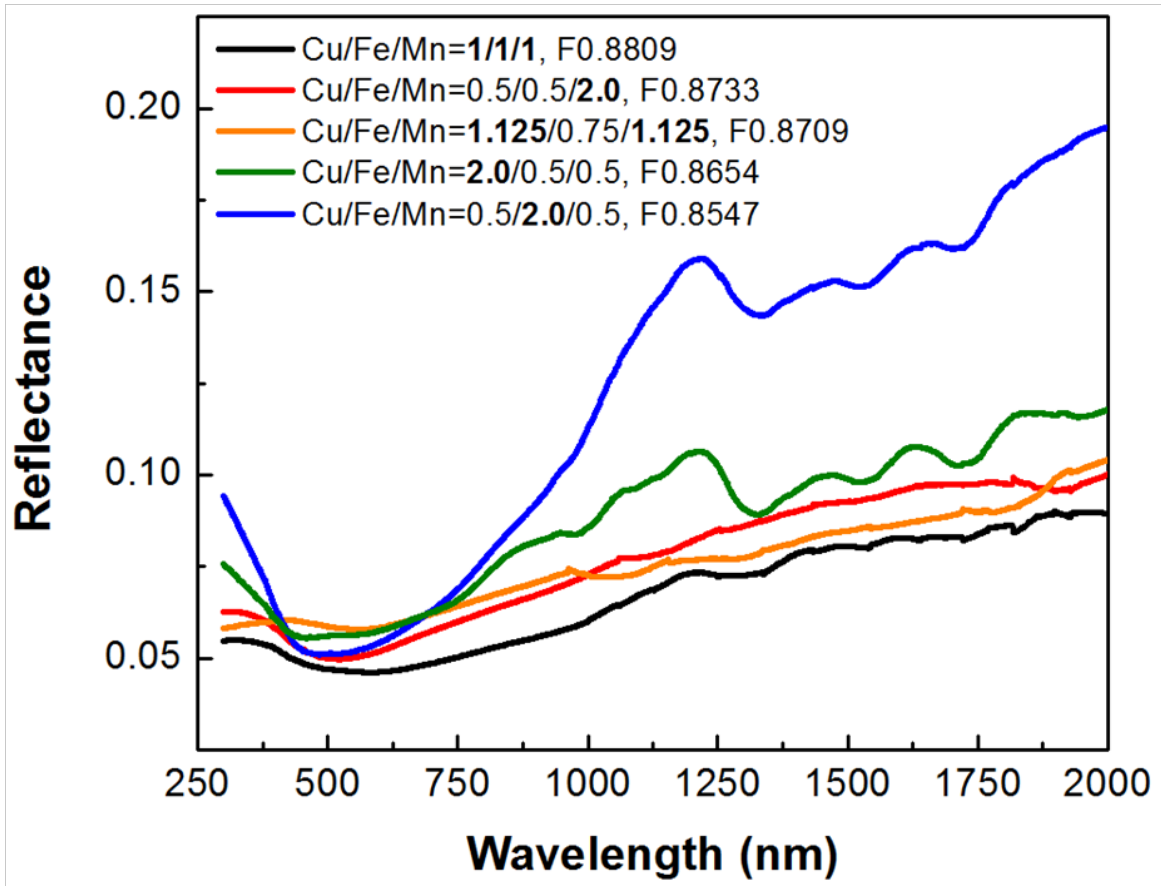
Fig. 8. Reflectance of SSC layers made of copper iron manganese particles with different atomic ratio (Cu/Fe/Mn). All samples had a dense single layer and were annealed with the condition of 750 ^{o}C/2h/air before reflectance measurement.

### 3.2.4 Ceramic Nano-Shell Effect

The refractory yttrium oxide (Y_2O_3) nano-shell was introduced as a new core-shell type structure. Such a structure coated with tight shell of very stable oxide like Y_2O_3 is expected to prevent nanoparticles from sintering-induced coarsening during high temperature service. Also, the presence of stable oxide shell could beneficially stabilize the oxidation state (oxygen deficiency or oxygen stoichiometry) of metal oxides much more than the oxide without a yttria shell. In order to confirm these effects of yttria shell, Fe_3O_4-Y_2O_3 core-shell nanoparticles were synthesized utilizing the concept of a reverse emulsion method which was previously applied for SiO_2 shell [6], with 20-30 nm Fe_3O_4 particles and $Y(O\text{-}iPr)_3$ (yttrium iso-propoxide) precursor, as the procedure described in **Fig. 9**.
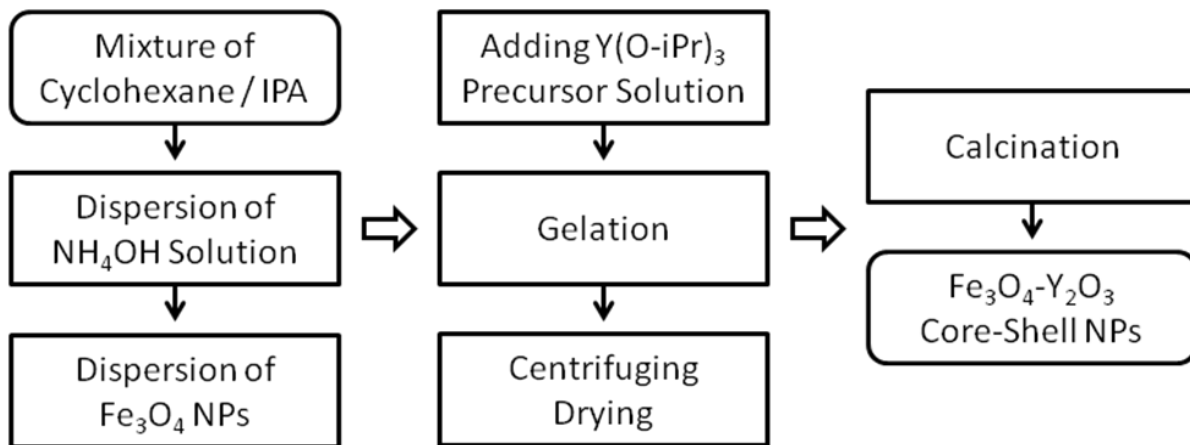
Fig. 9. The nano-shell synthesis procedure to make Fe_3O_4-Y_2O_3 core-shell NPs.

When the core-shell nanoparticle was observed with TEM, the core was Fe_3O_4 having (220) and (400) plane as a main crystal structure and the shell could be estimated to be Y_2O_3 which had (026), (541), (046), or (543), as shown in **Fig. 10** (c) and **Table 2**. The yttria shell is approximately 1-2 nm thick as seen in **Fig. 10** (a) and (b).
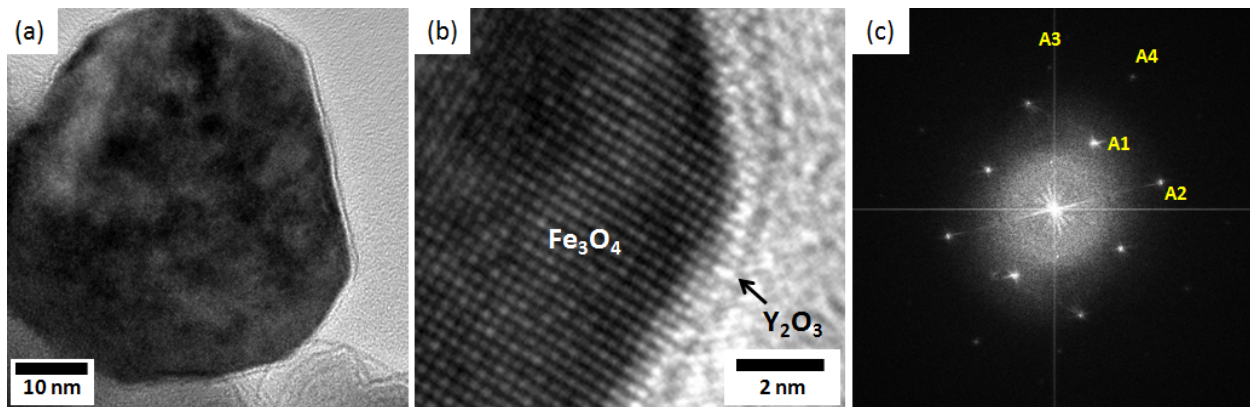
Fig. 10. (a) TEM images of Fe_3O_4-Y_2O_3 core-shell nanoparticles, (b) its magnified lattice image, and (c) its FFT patterns for the image (b).

Table 2. The possible crystal planes related to FFT patterns in Fig. 10 (c).

	d-spacing (Å)	Fe_3O_4 (Core)	Y_2O_3 (Shell)
A1	2.978	(220)	-
A2	2.099	(400)	-
A3	1.616	(511)	(026), (541)
A4	1.488	(440)	(046), (543)

The formation of yttria shell could be also confirmed by EDX analysis from which Y element occupied around 4 at% and Fe element was approximately 26 at%, as seen in **Fig. 11.**

Element	Weight%	Atomic%
O K	38.19	69.99
Fe L	49.32	25.89
Y L	12.50	4.12
Totals	100.00	
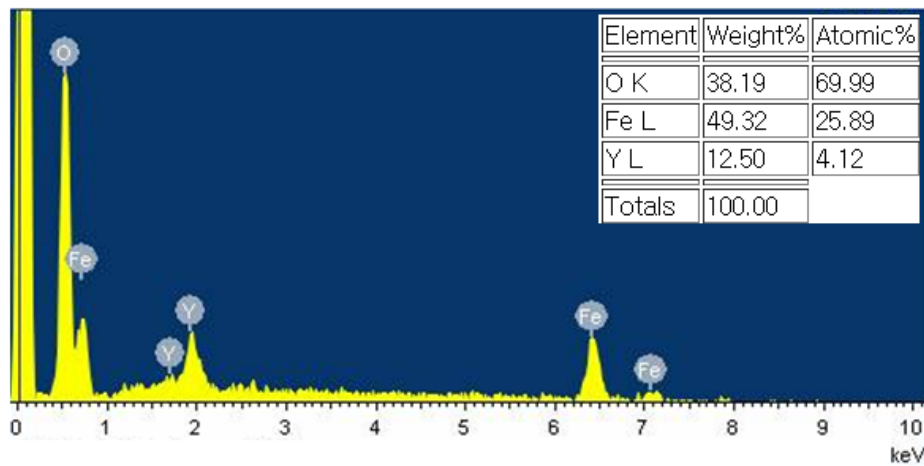
Fig. 11. EDX analysis result of Fe_3O_4-Y_2O_3 core-shell nanoparticles.

Yttria shell effect could be evaluated by comparing the sintered size between bare Fe_3O_4 NPs and Y_2O_3-coated Fe_3O_4 NPs, as shown in **Fig. 12**. From the result of annealing test, it was proved that yttria shell played a role of making the sintering of iron oxide core nanoparticles more difficult up to a temperature of 750°C. The nanoparticle sintering rate at 950°C was also reduced, as listed in Table 8.

This type of ceramic nanoshell can be applied for other metal oxide particles such as metal-ferrites, cobalt oxide, and copper oxide to keep particles from sintering and growing at high temperature. In addition to yttria shell, silica (SiO_2) shell can be considered to reduce the sintering phenomena and to increase the thermal stability of oxygen stoichiometry of metal oxides.

Y$_2$O$_3$-coated Fe$_3$O$_4$ NPs
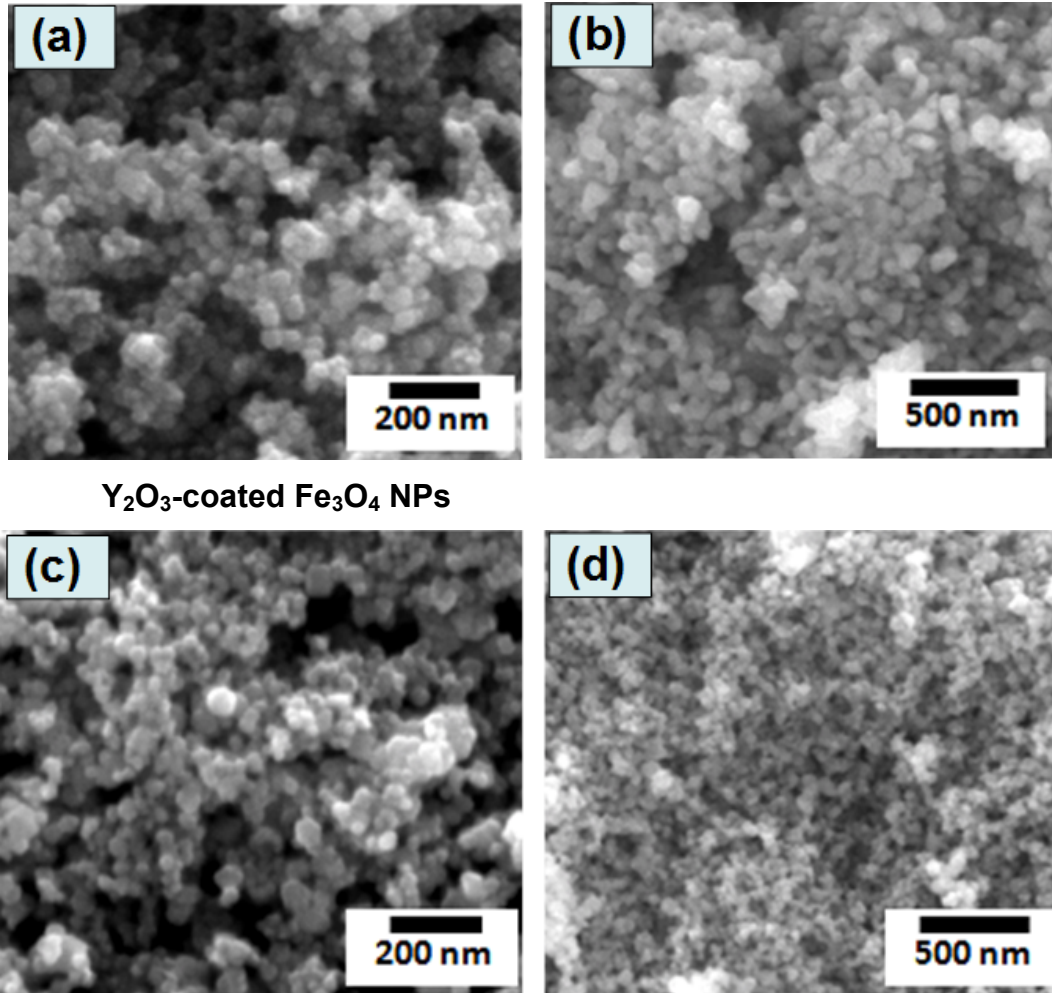
Fig. 12. SEM images showing the size change of bare Fe$_3$O$_4$ and Y$_2$O$_3$-coated Fe$_3$O$_4$ NPs depending on the annealing temperature. (a)~(b) : Fe$_3$O$_4$, (c)~(d) : Y$_2$O$_3$-coated Fe$_3$O$_4$, (a) and (c) : As-made, (b) and (d) : annealed at 750 ^{o}C for 2 hr.

Table 3. The summarized size change after annealing test at high temperature.

	As-made	**750 ^{o}C 2h Air**
Fe$_3$O$_4$ NPs	20-30 nm	50-100 nm
Fe$_3$O$_4$-Y$_2$O$_3$	20-30 nm	30-50 nm

3.3 Coating Procedure and Surface Enhancement

3.3.1 Coating procedure

The coating procedure of the sunlight absorbing coating layers is shown in **Fig.13**. At first, silicone resin was diluted with toluene (or xylene) and isobutanol (3:1) mixture in accordance with a designed recipe and homogenized thoroughly by using a ultrasonic probe for 30 mins. During sonication process, a container of the mixture was immersed in an ice bath to avoid the concentration change due to solvent evaporation. Then,

synthesized nano-sized powders were added into the diluted resin. In order to fabricate uniform slurries, a ball milling process was carried out. Yttria stabilized zirconia grinding balls with two different sizes (1/4" and 1/8" diameters, were mixed into the blend of powders and diluted resin by volume ratio 1:1. The ball milling process was performed for 24 hours. The slurry was obtained after sieving out YSZ balls using a poly mesh sheet. The Inconel substrates were prepared in advance with the following procedures. The surfaces of metal substrates were roughened via sandblasting. The Inconel coupons were cleaned via ultra-sonication in acetone and IPA for 30 mins. A gravity-feed air-brush was used for spraying the slurry on Inconel substrates. The spray conditions were optimized and the optima values are as follow: pressure: 40 psi, distance between the spray gun and the sample: 10 cm, and scan speed: 10 cm/sec. Finally, in order to convert the methyphenyl polysiloxane resin to SiO_2 dielectric matrix, the samples were cured at 250 ^{o}C in open air for 1hour on a hot plate.
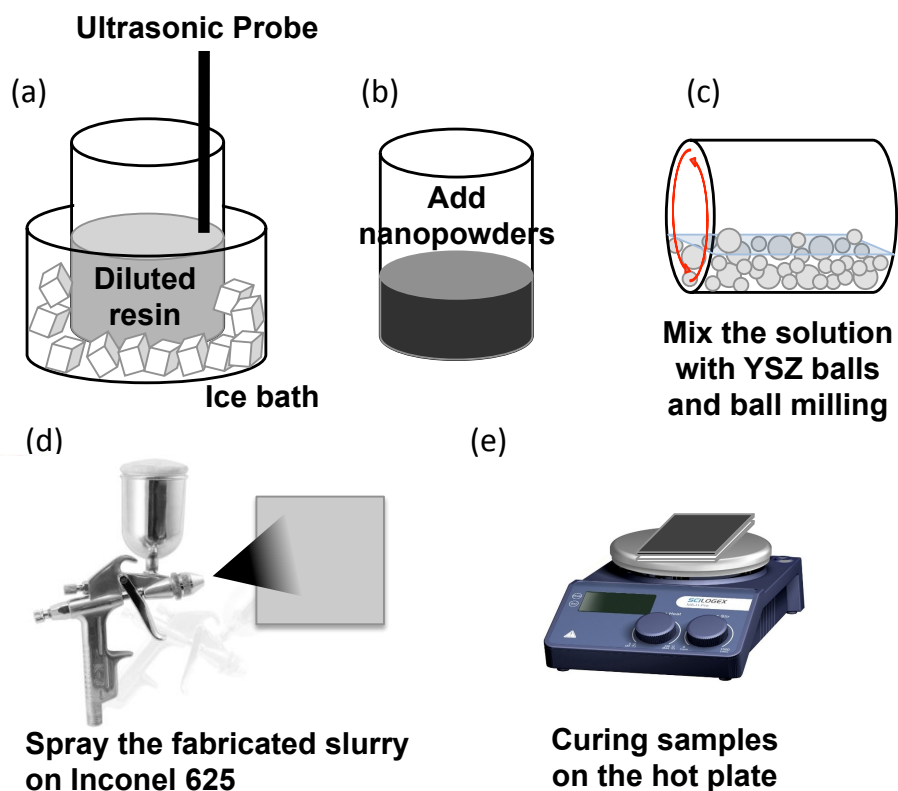
Fig 13. Fabrication procedure of light absorbing coating layers: (a) diluted resin with toluene(or xylnene) and isobutanol (volume 3:1) thoroughly using an ultra-sonic probe, (b) added the synthesized nanopowders into the diluted resin, (c) ball milled the slurry with zirconia grinding balls for 24hours, (d) sprayed the slurry on Inconel metal substrates and (e) cured the samples at 250°C for 1hour

3.3.2 Surface Roughness Enhancement

It is well known that a surface with proper roughness could possess enhanced solar absorption. The length scale most relevant to optical performance lies in 100s

nanometers to a few microns. In order to enhance the roughness of otherwise flat surfaces made from the spray coating process, here we employed polymer beads as sacrificial materials to create micron scale roughness.

We first aim to make porous coating structures by using sacrificial organic additives, such as polymer beads, which were initially mixed with the coating materials and subsequently removed upon high-temperature annealing, leaving behind voids that give rise to porous structures and rough surfaces. We applied commercially available polystyrene beads with controllable size distribution (other type of polymer beads should also be feasible). In order to make porous coating layers and enhance the surface roughness on black oxide coating samples, the volumetric concentration of the polymer beads, the black oxide powders, and SiO_2 matrix was optimized.

The detailed processes of making the porous & rough structures using the polymeric beads are as follows: (a) Mixing silicon resin and xylene and isobutanol (3:1) mixture by using probe-sonication for 30mins, (b) adding the polymer beads and the homogenization by using probe-sonication for 30min, (c) adding the black oxide powders into the solution, (d) ball milling with YSZ grinding balls for 24hours, (e) spraying the slurry on Inconel substrate, and (f) removing the polymer beads by heating the samples at 750°C for 30mins.

The enhanced surface roughness was observed in SEM images (**Fig. 14**(a)-(c)). As the volume of polymer beads increases, the surface gets roughened which leads light absorptivity. The reflectance results and the FOM are presented in Section 4.2.3.
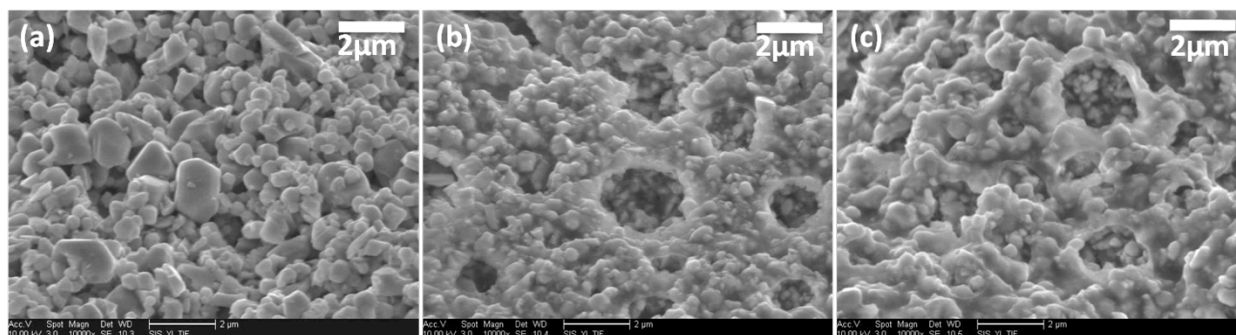
Fig. 14. SEM images of the porous Co3O4 layers employing the polymer with the polymer beads of volume ratio 1:2 and 1:3 were shown in (a)-(c), respectively.

3.3.3 Two-layer structure to achieve FOM of 0.9019

Various structures of SSC layer were tried to be fabricated on Inconel substrate including two double layered structures and one composite layer (mixture layer) using previously optimized copper chromite and copper iron manganese nanoparticles; a double layer of $CuFeMnO_4$ (porous top layer) / $CuCr_2O_4$ (dense bottom layer), a double

layer of $CuCr_2O_4$ (porous top layer) / $CuFeMnO_4$ (dense bottom layer), and a porous composite single layer of $CuCr_2O_4$ (70 wt%) + $CuFeMnO_4$ (30 wt%).

All SSC layers were annealed at 750 ^oC/2h/air before measuring reflectance. **Fig. 15** shows that the porous composite single layer structured SSC sample has lowest FOM value (0.8873) and the double layered SSC sample of $CuFeMnO_4$ (porous top layer) / $CuCr_2O_4$ (dense bottom layer) achieves **the best FOM value (0.9019)** which is higher than that of Pyromark (FOM=0.8968). From this research, we can determine the optimized layer structure to obtain better FOM of SSC layer and the thermal cycling and isothermal test will be applied to this double layered structure composed of $CuFeMnO_4$ (porous top layer) / $CuCr_2O_4$ (dense bottom layer).
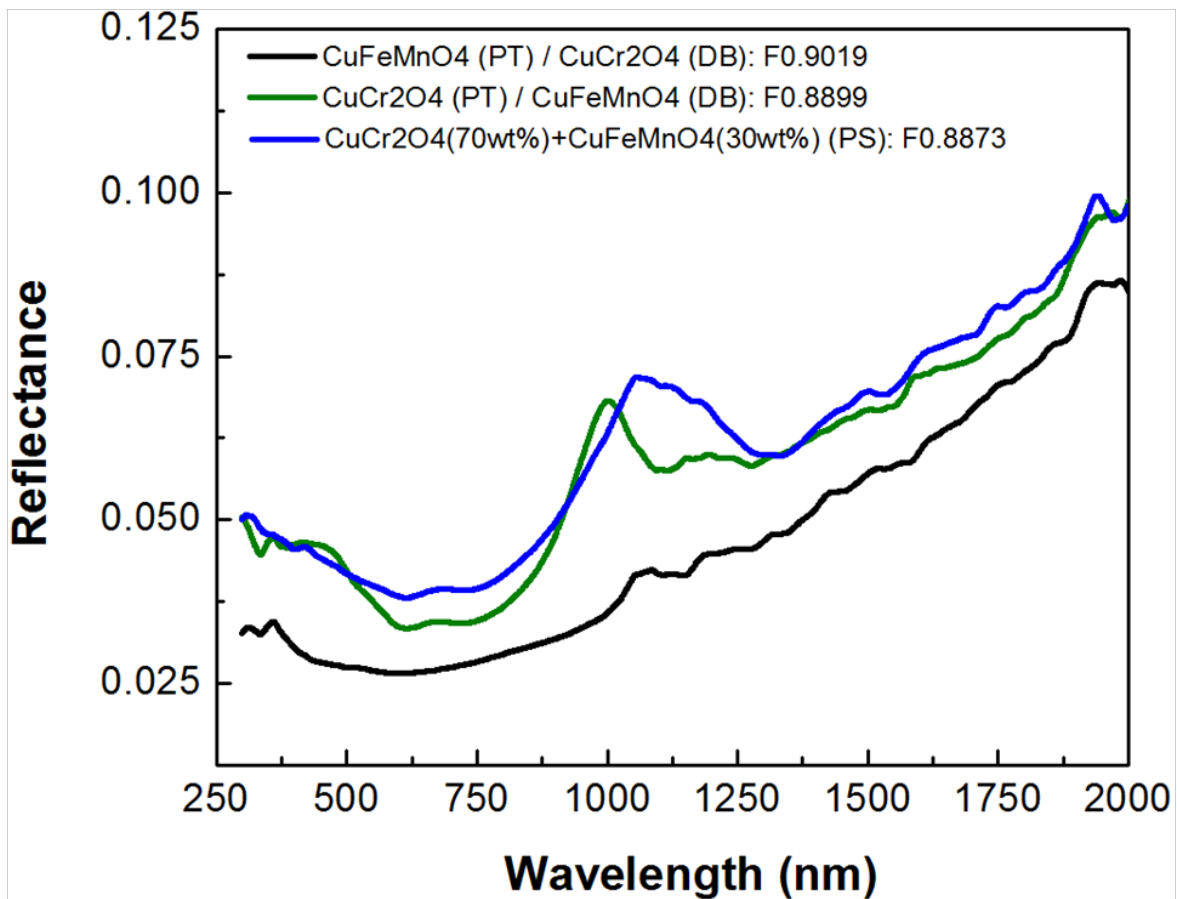
Fig. 15. Reflectance of double-layered sample and a single composite layered samples, fabricated with copper chromite and copper iron manganese oxide nanoparticles. All samples were annealed with the condition of 750 ^oC/2h/air before measuring. **PT**: porous top layer, **DB**: dense bottom layer, and **PS**: porous single layer.

The effect of the porous layer and double layered structures is shown in **Fig. 16**. In the case of single layered structure coated with $CuFeMnO_4$ particles, a porous single layered sample fabricated utilizing pore-forming polymer beads has much lower reflectance and a higher FOM (0.8945) than a dense single layered sample (FOM=0.8809) owing to the light trapping effect induced by the porous structure.

This porous $CuFeMnO_4$ layer has lower reflectance in visible spectrum but shows a little bit higher reflectance in near-IR (>1.1 μm) than $CuCr_2O_4$ dense single layer. And copper chromite layer has a disadvantage that it has higher reflectance of near-IR close to 1 μm which is a light with high energy relatively compared to IR with longer wavelength.

The double layered structure of $CuFeMnO_4$ (porous top layer) / $CuCr_2O_4$ (dense bottom layer) exhibits **the highest FOM (0.9019)** as show in **Fig. 16**. The porous $CuFeMnO_4$ top layer contributes to decrease reflectance in visible and near-IR around 1 μm spectrum. And the dense $CuCr_2O_4$ bottom layer plays a role of reducing reflectance in near-IR above 1.1 μm.
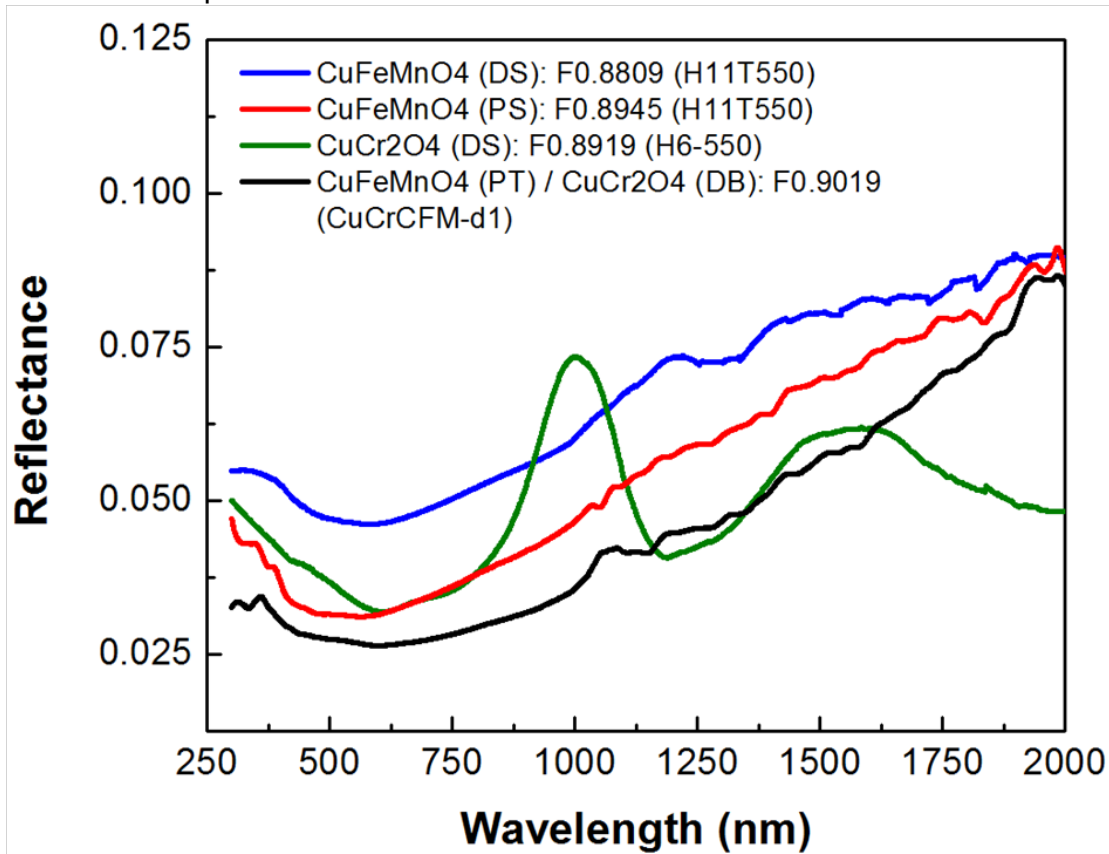
Fig. 16. Effect of porous layer structure and double layer on reflectance for SSC layers made of copper chromite particles and copper iron manganese particles. DS: dense single layer, PS: porous single layer, PT: porous top layer, and DB: dense bottom layer.

3.4 Characterization of the Solar Absorber Coatings

3.4.1 Coating Adhesion Evaluation of SSC layers (Tape Testing)

The coating adhesion quality was evaluated by ASTM standard D3359 tape testing method. Since the coating materials proposed in this project are inorganic, while ASTM Standard D3359[7] is designed for polymeric coating adhesion, a modified version of this standard was used to assess an adhesion property. Most of procedures followed

the standard except cutting procedure, because unlike organic coatings, the coating layer of oxide powder in SiO_2 matrix is not flexible and is brittle. Test method B that is more suitable for use in the laboratory was applied in our tests. The size of coupons is 0.5 x 0.5 inch. For this test, 3M-600 pressure sensitive tape was used and this tape is a recommended one to use for another standard method (IPC-TM-650). The adhesion to steel is 40oz./in according to the information from 3M.

At first, the center of the tape was placed on the sample and in the area of the sample smooth into place by a finger. To make sure good contact with the film, the tape was firmly rubbed with the eraser and the cotton swaps. We checked the color change that is a good indicator when the good contact was made. Within 1min of application, we removed the tape by seizing the free end and rapidly back upon itself at as close to an angle of 180° as possible. And then, the tapes and the samples after tape testing were inspected carefully by naked eyes and optical microscope. To get the portion of the lost area, we performed an image processing on the photographs of the tapes.

3.4.2 Measurement of Figure of Merit

As shown in Fig.1, one of the objectives of this project is to achieve a thermal efficiency, as measured by figure of merit (FOM), to a very high level of 90%. The FOM for the prepared coatings is defined as:

$$F = \frac{\int_0^\infty (1-R(\lambda))I(\lambda)d\lambda - \frac{1}{C}\left[\int_0^\infty (1-R(\lambda))B(\lambda,T)d\lambda\right]}{\int_0^\infty I(\lambda)d\lambda} \qquad (1)$$

where R(λ) is the measured spectral selectivity, I(λ) is the spectral solar radiance per square meter as defined by ASTM G173, B(λ,T) is the spectral thermal emission of a black body, and C is the concentration ratio (number of suns, or ratio of reflector area to absorber area). The temperature of the receiver (and therefore black body) is assumed to be 750°C. In practice, all integrals are evaluated in the range of [300nm-20um], as only negligible quantities of solar power are present outside this range.

Reflection data is collected using a Labsphere® 4" integration sphere and Andor® 303i spectrometer equipped with a Si based (spectral range 300-1100nm) and InGaAs based (spectral range 900nm-2500nm) detector. Reflection behavior of samples beyond 2.5um is extrapolated.A 4" LabSphere® integration sphere (Fig. 17) was used to collect all angles of reflection from test samples. Incident illumination angle was 12.5° +/- 2.5° (conical focus). Illumination spot size was controllable via an aperture in the beam path and was typically 15mm in diameter. Spectra are analyzed using an Andor® 303i spectrometer equipped with Newton (Si based, range 300-1100nm) and iDus (InGaAs based, range 900-2500nm) detectors. Illumination was produced from a tungsten halogen lamp.
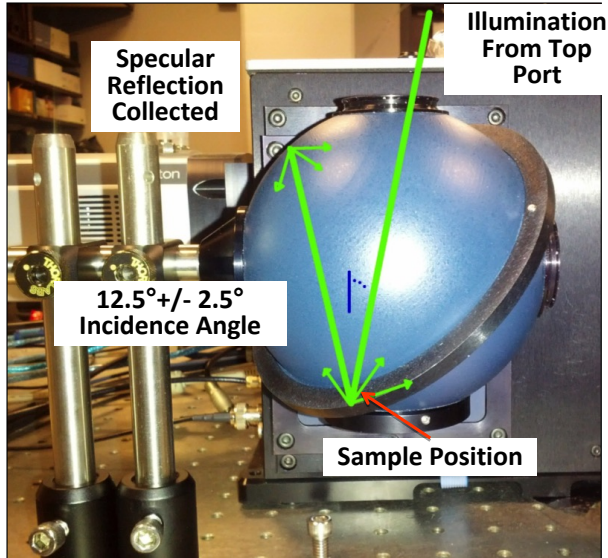
Fig. 17. Integration sphere configuration. Light is incident through top port onto sample resting at bottom port. Incidence is controlled to retain specular component of reflection.

In order to evaluate high temperature emission from samples, a custom heated stage was constructed and integrated with a Matteson Galaxy 5020 Fourier transform infrared spectrometer (FTIR) (Fig. 18). The resistively heated sample replaced the system lamp as the IR light source. In order to reduce heat loss, the samples were kept under vacuum. The collected sample emission was normalized to that from a test pyromark sample and then absolute emissivity obtained by referencing the literature reported value for Pyromark spectral emissivity [8].
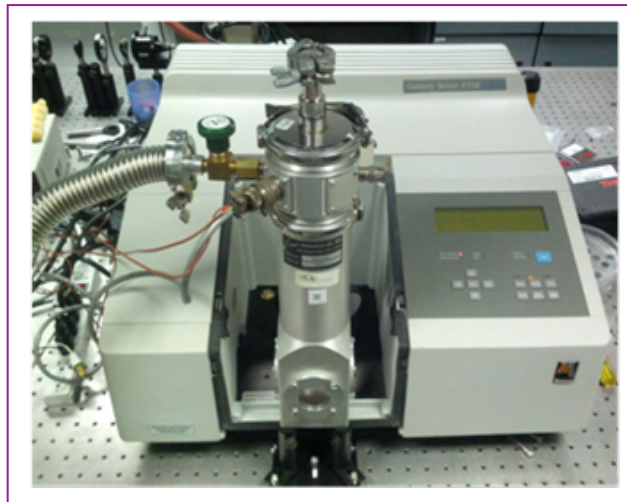
Fig. 18. High temperature stage integration into Mattson® based FTIR system.

4   Project Outcomes and Discussions

Based on the results shown in the previous sections, porous structures were optimized with various polymer beads composition and 2-layered tandem structure was devised using **a porous CuFeMnO$_4$ top layer and a dense CuCr$_2$O$_4$ bottom layer**, by which the higher FOM could be obtained (**FOM=0.9019**), compared to FOM=0.895 for Pyromark samples that were coated at UCSD using identical procedures as well as FOM=0.871 for Pyromark samples obtained directly from a CSP company. Therefore, **we have developed a SSC material with a FOM greater than 0.90, which meets the FOM milestone required by DOE.**

Herein, we will present our results on durability tests and various other studies on SSC samples made from the same materials and processes, namely, a porous CuFeMnO$_4$ top layer and a dense CuCr$_2$O$_4$ bottom layer (referred to as "CFM(PT)/CuCr2O4(DB) samples" hereafer). These tests include adhesion tests, FOM endurance tests after isothermal annealing and thermal cycling, reparability tests. As we will show later, **our new CFM(PT)/CuCr2O4(DB) samples can meet all the milestones set by DOE, which is not possible in Pyromark.**

4.1   FOM Endurance after Thermal Testing

SunShot milestone: FOM endurance ($\geq$ 0.98) & high FOM value (>Pyromark) after isothermal annealing and thermal cyclings test in air atmosphere.

As shown in Table 4, four samples were evaluated for FOM endurance test. 2-layered tandem structure was fabricated with a porous CuFeMnO4 (CFM) layer and a dense CuCr2O4 layer (so called "CFM(PT)/CuCr2O4(DB)"). Another 2-layered structure was made of a porous Co3O4 top layer with a dense Co3O4 bottom layer. Lab-coated Pyromark sample was fabricated with a modified Pyromark paint diluted by additional solvent (Xylene/Toluene). CSP company's Pyromark sample was made by CSP company using their Pyromark paint and coating method.

Table 4. Samples applied for FOM endurance evaluation.

CFM(PT)/CuCr2O4(DB)	Co3O4(PT)/Co3O4(DB)	Pyromark (DS) (Lab-Coated)	Pyromark (CSP Company)
synthesized NPs-solution-coating	synthesized NPs-solution-coating	commercial paint-modified w/ solvent	commercial paint-coated by CSP comp.

(PT: porous top layer, DB: dense bottom layer, DS: dense single layer)

Four types of thermal durability tests were carried out in air environment including thermal cycling (RT to 600°C for 100cycles, RT to 750°C for 100cycles) and isothermal annealing test (at 600°C for 1000h, at 750°C for 500h) as temperature profiles shown in

Fig. 19. The thermal cycling was made so fast that samples could be affected by large thermal shock which could bring cracks and delamination problem. Here, the FOM endurance is defined as the ratio of the FOM value after thermal tests to that of before the tests.

(a)   (b)

Isothermal Annealing Test

$$\frac{FOM[t = 500h; 750C]}{FOM[t = 0; 750C]} \qquad \frac{FOM[t = 1000h; 600C]}{FOM[t = 0; 600C]}$$

Temperature

a. 750°C/500h

b. 600°C/1000h

5°C/min   air cooling

in Air

Time

Rapid Thermal Cycling Test

$$\frac{FOM[n = 100; 25\ to\ 750C]}{FOM[n = 1; 25\ to\ 750C]} \qquad \frac{FOM[n = 100; 25\ to\ 600C]}{FOM[n = 1; 25\ to\ 600C]}$$

Temperature

c. 750°C / d. 600°C

+150°C/min   -150°C/min

in Air

Time
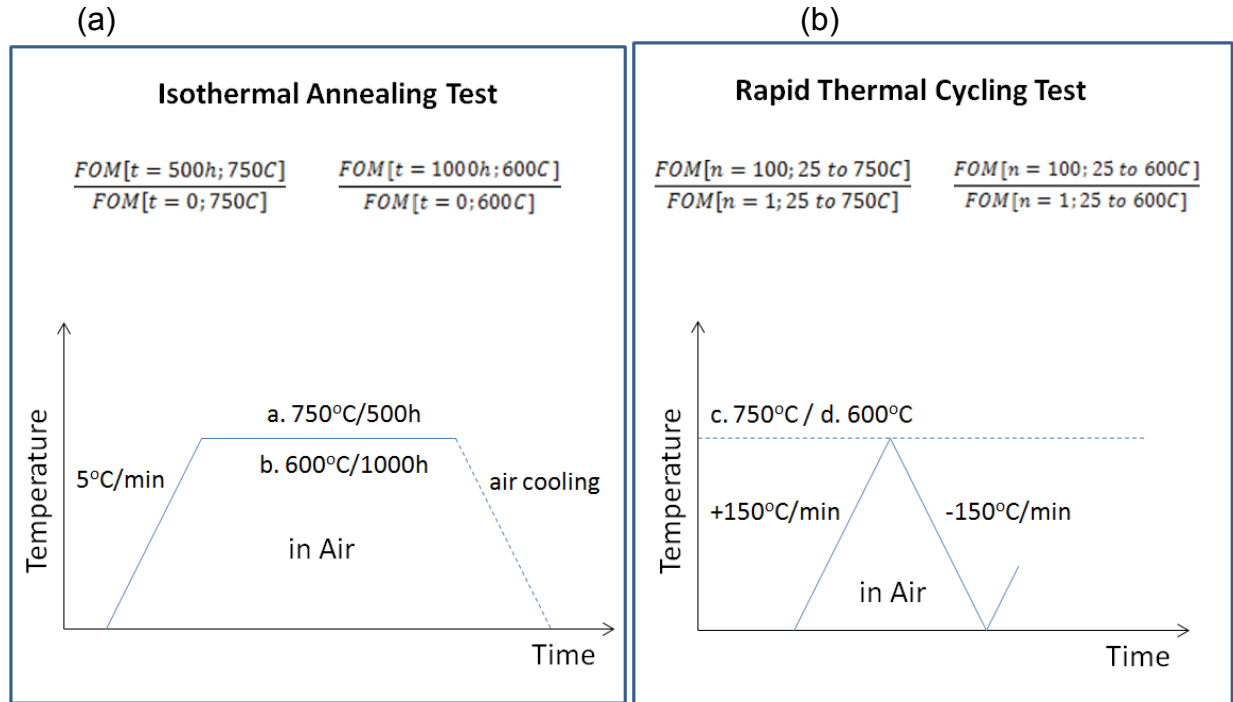
Fig. 19. Temperature profiles for (a) isothermal annealing test and (b) rapid thermal cycling test, and the equation to calculate FOM endurance.

4.1.1 600°C Thermal Cycling Test (RT-600°C/100cycles/Air)

CuFeMnO4(PT)/CuCr2O4(DB), Co_3O_4(PT)/Co_3O_4(DB), and Lab-Coated Pyromark(DS) were tested with thermal cycling (RT-600 ^{o}C/100cycles) in air.

Fig. 20 shows the reflectance measured after 1 cycle and 100 cycles thermal cycling test. The Co_3O_4(PT)/Co_3O_4(DB) sample and lab-coated Pyromark sample showed increased reflectance in spectrum from VIS to 1um and decreased reflectance near 2 um, which reduced their FOM values after thermal cycling. On the other hand, the CFM(PT)/CuCr2O4(DB) sample after 100 cycles showed slightly reduced reflectance in THE visible spectrum and possessed similar reflectance near 2um, which led to a high FOM endurance value after cycling, as shown in Table 5.
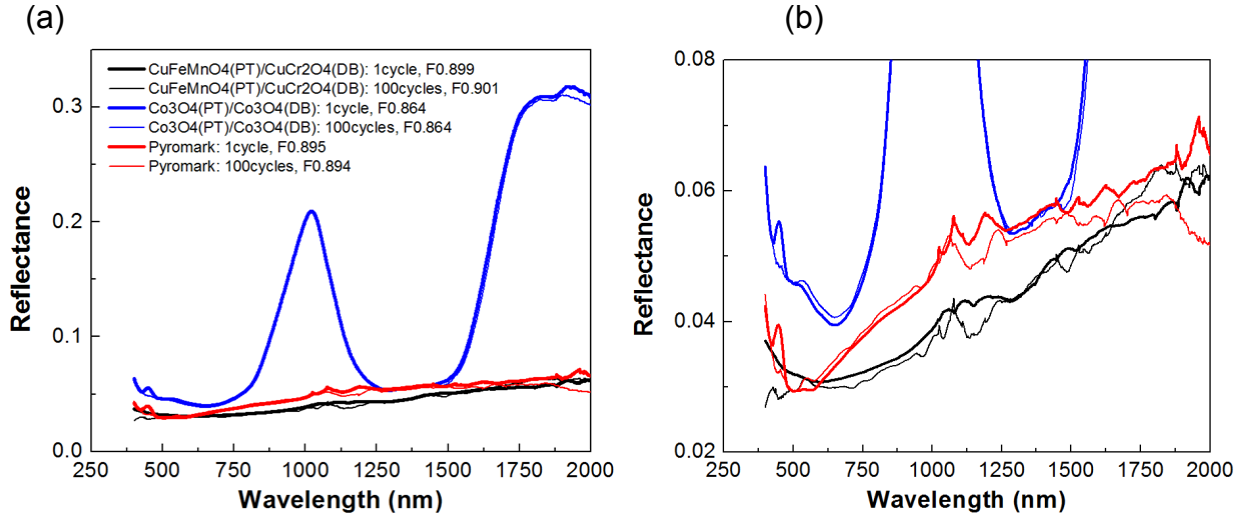
Fig. 20. Comparison of reflectance and FOM between 1-cycled samples and 100-cycled samples from RT to 600°C in air. (PT: porous top layer, DB: dense bottom layer)

As summarized in Table 5, all the three types of samples **satisfied the goal of FOM endurance (≥0.98)** after the thermal cycling tests. Additionally, table 6 shows t-test results with which minimum value of FOM can be calculated in 95% confidence. Our CFM(PT)/CuCr2O4(DB) sample also possess a higher FOM value compared to Pyromark after the thermal cycling. **Therefore,** the CFM(PT)/CuCr2O4(DB) sample satisfies **both the requirements of a high FOM value and high FOM endurance.**

Table 5. FOM endurance after thermal cycling (RT-600°C/100cycles/air), based on mean values and minimum values in 95% confidence.

|	1 cycle	100 cycles (mean)	100 cycles (min. 95% conf.)	FOM Endurance (w/ mean)	FOM Endurance (w/ min.)
CFM/CuCr2O4	0.899	0.898	0.897	**0.9989**	**0.9978**
Co3O4/Co3O4	0.864	0.860	0.860	**0.9954**	**0.9954**
Pyromark (Lab)	0.895	0.892	0.890	**0.9966**	**0.9944**

Table 6. t-test of FOM values obtained from reflectance measurements after thermal cycling (RT-600°C/100cycles/air).

t-test	CFM/CuCr2O4	Co3O4/Co3O4	Pyromark (Lab-Coated)
1	0.8973	0.8598	0.8899
2	0.8981	0.8597	0.8921

3	0.8986	0.8598	0.8926
4	0.8994	0.8602	0.8935
5	0.8984	0.8600	0.8931
Mean Value	**0.89836**	**0.85990**	**0.89224**
Std Deviation	0.00076354	0.0002	0.00140996
95% Conf. Min.	**0.89741209**	**0.85965171**	**0.89048958**

4.1.2 600°C Isothermal Annealing Test (600°C/1000h/Air)

Fig.21 shows that both CuFeMnO4/CuCr2O4 sample and lab-coated Pyromark sample have a similar behavior that reflectance increased slightly in visible spectrum and decreased near 2um spectrum, by which FOMs of both samples were reduced after isothermal annealing at 600 °C/1000h/air. Co3O4/Co3O4 sample has better optical stability in visible spectrum after this isothermal test.
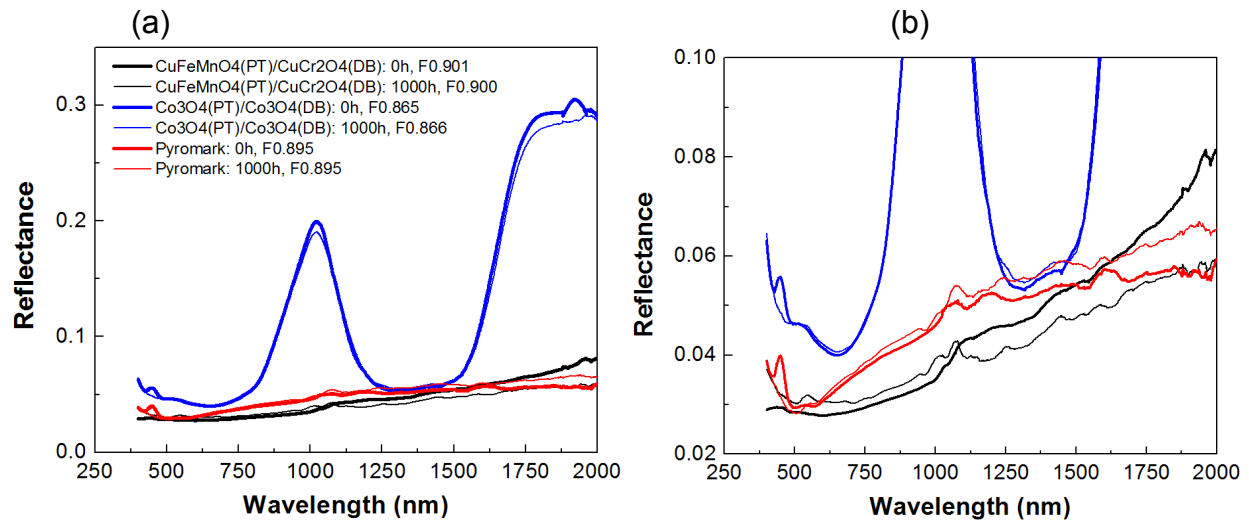
Fig. 21. Comparison of reflectance and FOM between as-prepared samples (0h) and samples annealed at 600°C/1000h/air. (PT: porous top layer, DB: dense bottom layer)

FOM endurance shown in Table 7 was evaluated based on t-test in Table 8. **All 3 samples satisfy SunShot milestones on the FOM endurance (≥0.98)**. Again, the **CFM(PT)/CuCr2O4(DB) sample also satisfies the high FOM goal (namely, greater than that of Pyromark).**

Table 7. FOM endurance after isothermal annealing at $600^{o}C/1000h/air$, based on mean values and minimum values in 95% confidence.

	0h	1000h (mean)	1000h (min. 95% conf.)	FOM Endurance (w/ mean)	FOM Endurance (w/ min)
CFM/CuCr2O4	0.901	**0.899**	0.898	**0.9978**	0.9967
Co3O4/Co3O4	0.865	**0.863**	0.862	**0.9977**	0.9965
Pyromark (Lab)	0.895	**0.893**	0.893	**0.9978**	0.9978

Table 8. T-test of FOM values obtained from reflectance measurements after isothermal annealing ($600^{o}C/1000h/air$).

t-test	CFM/CuCr2O4	Co3O4/Co3O4	Pyromark (Lab-Coated)
1	0.8979	0.862	0.8928
2	0.8986	0.8618	0.8931
3	0.8987	0.8633	0.8935
4	0.8989	0.8626	0.8934
5	0.8987	0.8631	0.8936
Mean Value	**0.89856**	**0.86256**	**0.89328**
Std Deviation	0.00038471	0.00065803	0.00032711
95% Conf. Min.	**0.8980824**	**0.86174308**	**0.89287391**

Fig. 22 displays photos of samples after thermal cycling and isothermal annealing at $600^{o}C/air$. There was no delamination problem in all the samples, including lab-coated Pyromark (adhesion property was evaluated by ASTM standard tape testing as described before, and the results are shown as a milestone in the next sections).
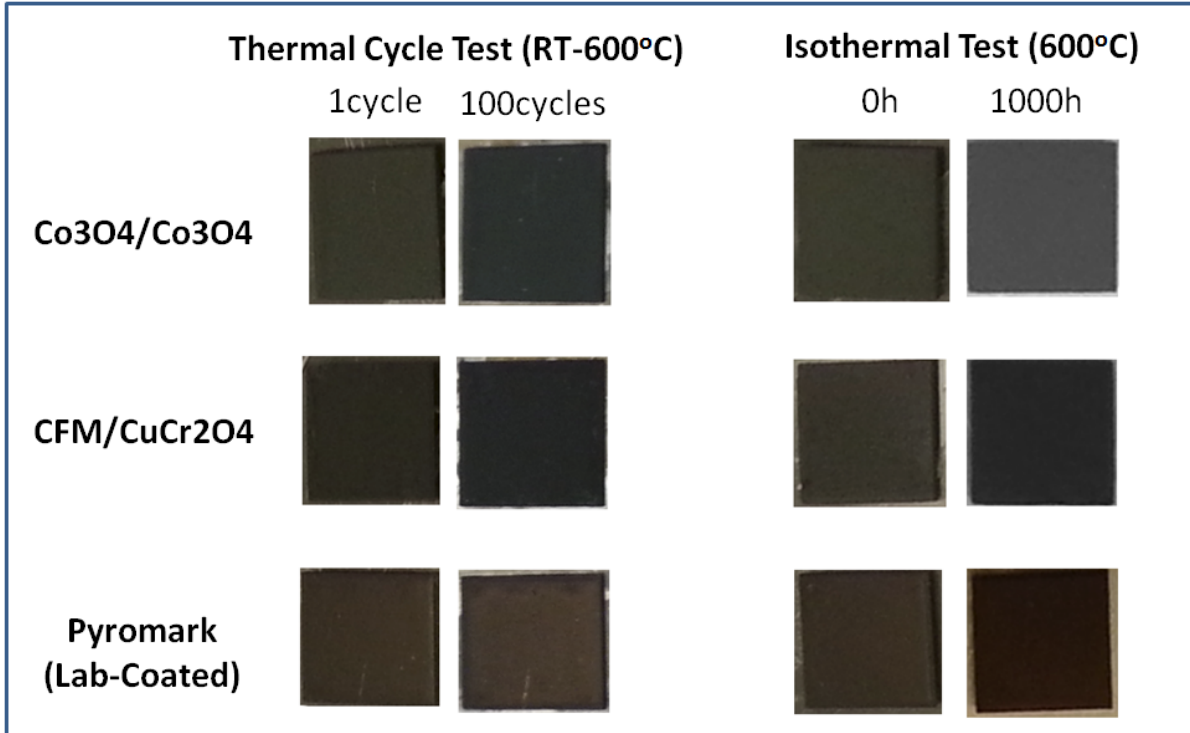
Fig.22. Photos of samples after thermal cycling (left two columns) and isothermal annealing (right two columns) at 600°C in air. Surface color of the images can be different from real colors because photos were not taken under the same environment.

4.1.3 750°C Thermal Cycling Test (RT-750°C/100cycles/Air)

In this thermal cycling test, CSP company-made Pyromark sample was included and compared to lab-coated Pyromark sample, which was fabricated with commercial Pyromark paint at UCSD by mixing additional solvents. Lab-coated Pyromark and our other samples were fabricated by spray coating. However, we did not know exactly the preparation procedure of the CSP company-made Pyromark sample.

Fig. 23 shows that the reflectance of the samples after the thermal cycling from RT to 750° in air for 100 cycles. Both the CFM(PT)/CuCr2O4(DB) and the lab-coated Pyromark samples showed increase in reflectance in the visible spectrum and decrease in the near-IR spectrum above 1 um. The reflectance increment in the visible spectrum can be induced by the reduction of surface porosity or roughness due to high temperature annealing. But dominant factors affecting the reflectance decrease in near-IR above 1um have to be studied in more details in future research. And CSP company-made Pyromark sample increased reflectance much more in all spectrum range.

(a)

(b)
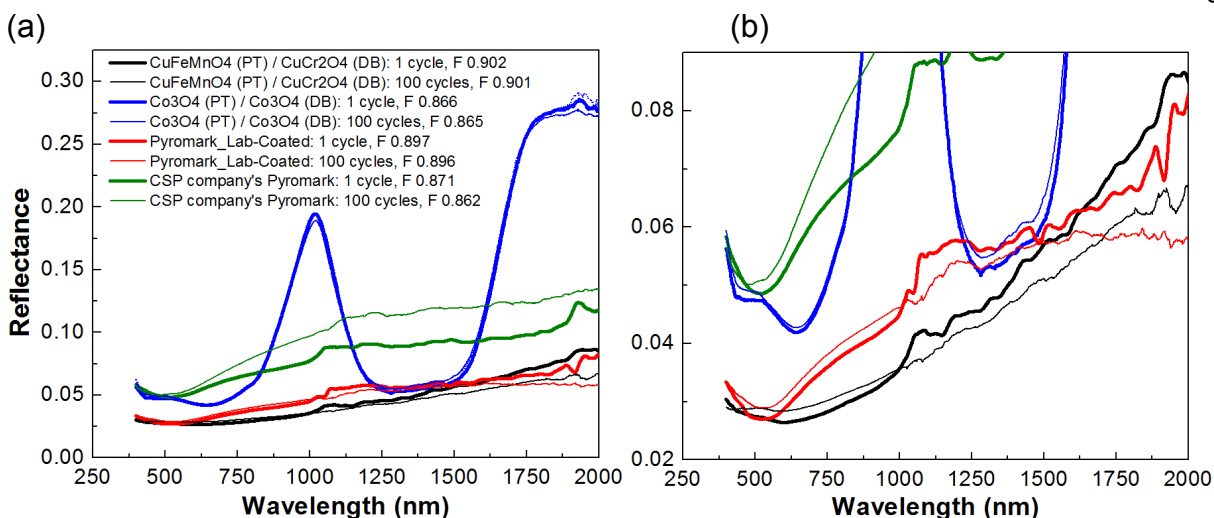
Fig. 23. Comparison of reflectance and FOM between 1-cycled samples and 100-cycled samples from RT to 750°C in air. (PT: porous top layer, DB: dense bottom layer)

As shown in Table 9, **all 4 types of samples satisfy FOM endurance goal (≥0.98).** Again, the **CFM(PT)/CuCr2O4(DB) sample can reach both FOM endurance and a higher FOM value than Pyromark after thermal cycling**. The CSP company-made Pyromark sample has the lowest FOM endurance that can be caused by delamination as seen in **Fig. 24**. This delamination can expand from many micro cracks in the coating layer of the CSP company-made Pyromark sample that was observed in **Fig. 25** (d-2). When there are many cracks, reflectance can increase because spectrum can pass through cracks and reach Inconel substrate on which spectrum can be reflected more than SSC layer.

Table 9. FOM endurance after thermal cycling (RT-750°C/100cycles/air), based on mean values and minimum values in 95% confidence.

	1 cycle	10 cycles	100 cycles (mean)	100 cycles (min.)	FOM Endurance (w/ mean)	FOM Endurance (w/ min.)
CuFeMnO4 / CuCr2O4	0.902	0.901	**0.901**	0.901	**0.9989**	**0.9989**
Co3O4 / Co3O4	0.866	0.865	**0.865**	0.865	**0.9988**	**0.9988**
Pyromark (Lab)	0.897	0.897	**0.895**	0.895	**0.9978**	**0.9978**
Pyromark (CSP Company)	0.871	0.871	**0.858**	0.854	**0.9851**	**0.9805**

Table 10. t-test of FOM values obtained from reflectance measurements after thermal cycling (RT-750°C/100cycles/air).

t-test	CFM/CuCr2O4	Co3O4/Co3O4	Pyromark (Lab-Coated)	Pyromark (CSP Company)
1	0.9013	0.8654	0.8952	0.8513
2	0.9014	0.8664	0.8958	0.8584
3	0.9010	0.8649	0.8957	0.8598
4	0.9007	0.8656	0.8956	0.8616
5	0.9010	0.8649	0.8946	0.8584
Mean Value	**0.90108**	**0.86544**	**0.89538**	**0.8579**
Std Deviation	0.000248193	0.000553534	0.00044	0.003503141
95% Conf. Min.	**0.90077**	**0.86475**	**0.89483**	**0.85355**
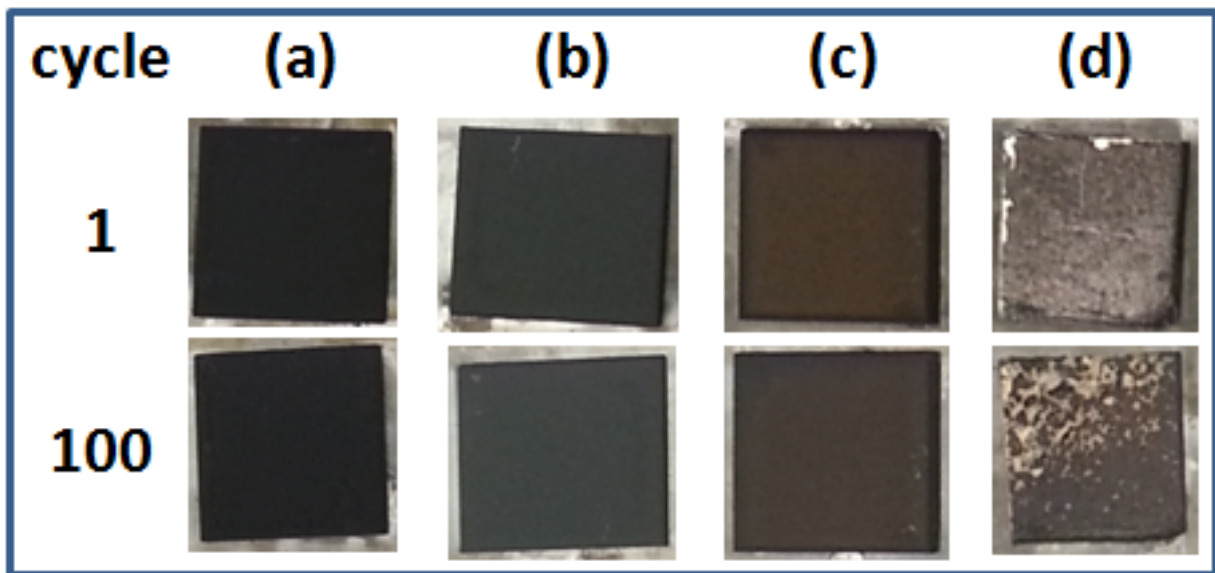
Fig. 24. Photo observation for 4 types of samples including CSP company-made Pyromark sample, taken after thermal cycling test (RT-750°C/100cycles/air).

After thermal cycling test (RT-750°C/100cycles/air), porous surface morphologies of CuFeMnO4/CuCr2O4 sample and Co3O4/Co3O4 sample were preserved well to be similar to 1-cycled samples in miro-scaled image, as can be seen in **Fig. 25** (a-1), (a-2), (b-1) and (b-2). These two-layered samples contain both nano-porous and micro-porous surface structure, which can decrease reflectance in both visible and near-IR spectrum. Nano-scaled morphology change can be studied in future research to analyze the effect of morphology change on reflectance through thermal tests in more details.

When evaluating the porous structure based on these SEM images, lab-coated Pyromark and CSP company-made Pyromark sample has much more dense surface structure than CuFeMnO4/CuCr2O4 sample and Co3O4/Co3O4 sample, as shown **Fig. 25** (c-1), (c-2), (d-1) and (d-2). Pyromark samples contain only very small nanopores on surface which cannot decrease reflectance in wide spectrum including visible and near-IR spectrum. Especially CSP company-made Pyromark sample has the most dense surface structure which is less effective to damp volume change during temperature change and can bring about many micro-cracks like inset image in **Fig. 25** (d-2) and finally the delamination problem that CSP companies are suffering from.
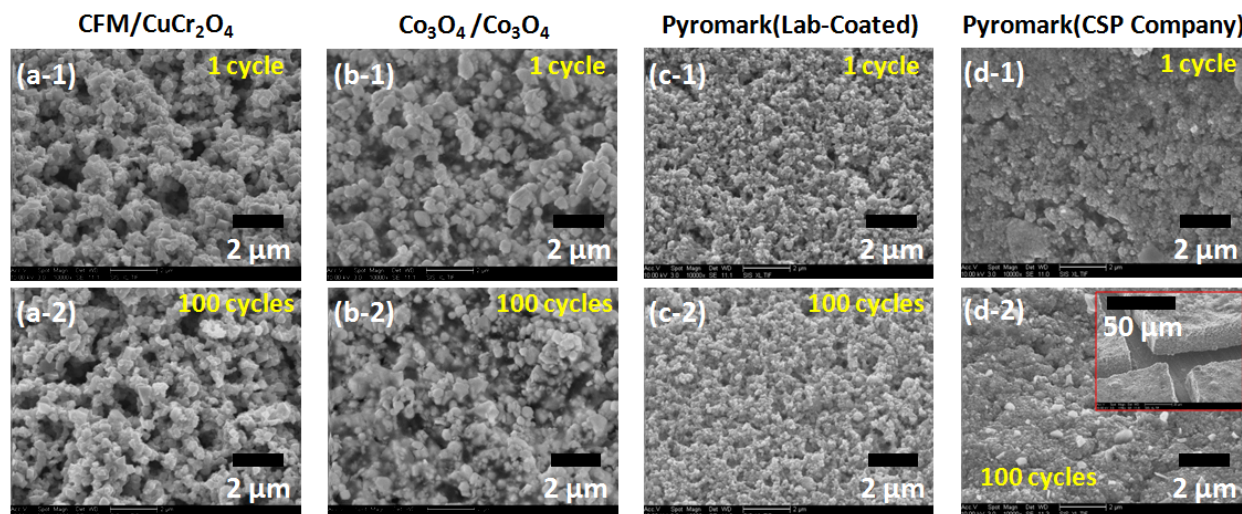

Fig. 25. SEM images showing surface morphologies of samples after 1 cycle and 100 cycles in thermal cycling (RT-750°C/air), and observed in tilted angle of 30 degree.

4.1.4 750°C Isothermal Annealing Test (750°C/500h/Air)

CSP company-made Pyromark sample was not placed for this isothermal test because it has the delamination problem that cannot make uniform measurement. Fig. 26 shows that all samples increased reflectance in wide spectrum range including visible spectrum and near-IR spectrum, which can be affected much by the most harsh thermal test conditions (750°C/500h/air). For instance, the porous surface morphology with nano-scaled pores and micro-scaled pores can be degraded at high temperature (750°C) for 500h, which can contribute to increase the reflectance in wide spectrum.

As shown in Fig. 26(b), in CuFeMnO4/CuCr2O4 sample and lab-coated Pyromark sample 1um peak emerged after isothermal annealing at 750°C. This new 1 um peaks may result from the new formation of CuO phase after a long time annealing at high temperature, because the layer made of CuO nanoparticles increases reflectance in near-IR spectrum from 800 nm wavelength, as shown in Fig. 27. The reason of 1 um reflectance peak has to be studied in future research.

(a)

(b)
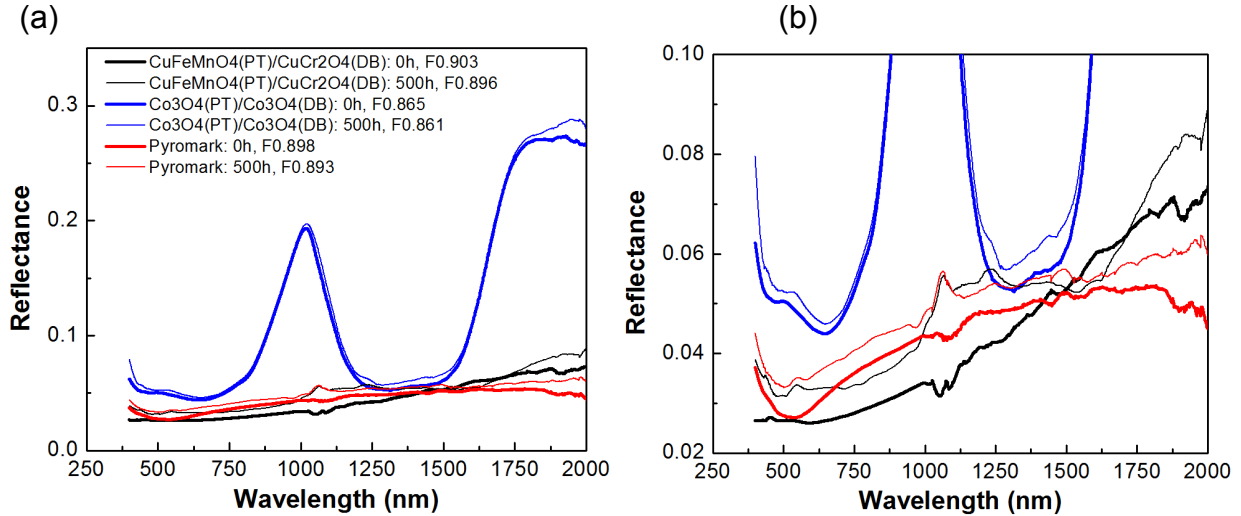
Fig. 26. Comparison of reflectance and FOM between as-prepared samples (0h) and samples annealed at 750°C/500h/air. (PT: porous top layer, DB: dense bottom layer)
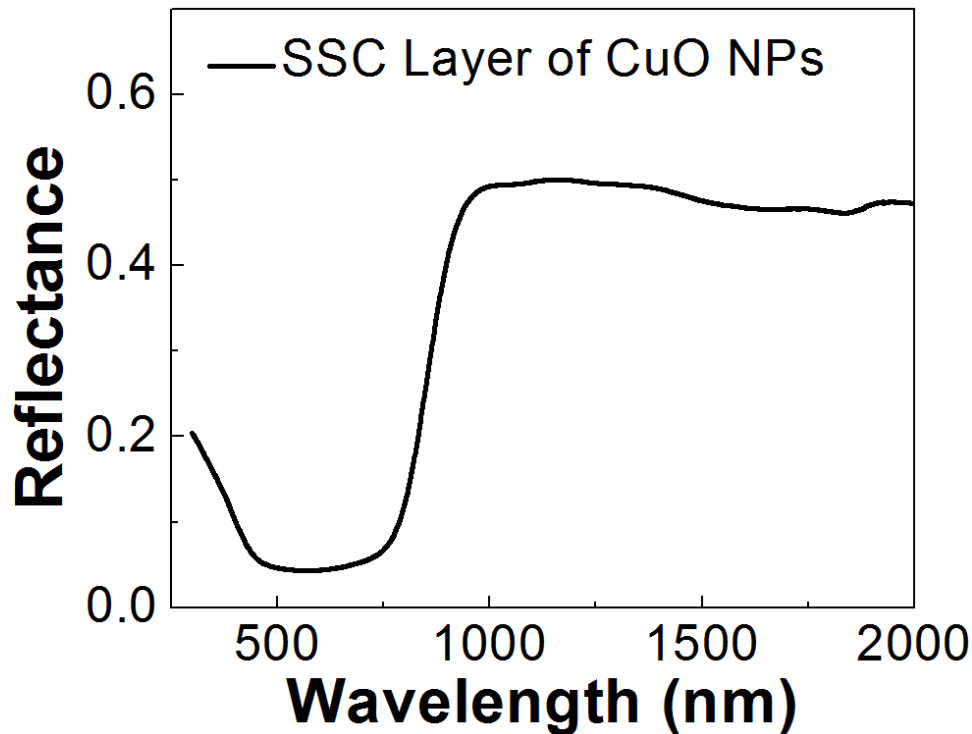
Fig. 27. Reflectance measured for SSC layer fabricated with CuO nanoparticles and annealed at 750°C/2h/air.

In Table 11, all samples satisfy FOM endurance goal but **only CuFeMnO4/CuCr2O4 sample can satisfy both FOM endurance (0.98) and high FOM goal (>Pyromark)**. That is, after the harshest isothermal test at 750°C for 500h in air, FOM of CuFeMnO4/CuCr2O4 sample still keeps 0.895 and 0.896.

Table 11. FOM endurance after isothermal annealing at 750°C/500h/air, based on mean values and minimum values in 95% confidence.

	0h	500h (mean)	500h (min. 95% conf.)	FOM Endurance (w/ mean)	FOM Endurance (w/ min)
CFM/CuCr2O4	0.903	**0.896**	0.895	**0.9922**	**0.9911**
Co3O4/Co3O4	0.865	**0.859**	0.858	**0.9931**	**0.9919**
Pyromark (Lab)	0.898	**0.893**	0.892	**0.9944**	**0.9933**

Table 12. t-test of FOM values obtained from reflectance measurements after isothermal annealing (750°C/500h/air).

t-test	CFM/CuCr2O4	Co3O4/Co3O4	Pyromark (Lab-Coated)
1	0.8956	0.8583	0.8922
2	0.8955	0.8589	0.8923
3	0.8954	0.8592	0.8932
4	0.8964	0.8586	0.893
5	0.8955	0.8584	0.8941
Mean Value	**0.89568**	**0.85868**	**0.89296**
Std Deviation	0.00040866	0.00037014	0.00077006
95% Conf. Min.	**0.89517267**	**0.85822049**	**0.89200399**

After the isothermal annealing at 750°C/500h/air, the porous surface structure was almost preserved but the particle growth could be observed as shown in Fig. 28(b)-CuFeMnO4/CuCr2O4. This growing of particle and crystal can reduce the degree of surface porosity, by which reflectance can increase in all spectrum range. In lab-coated Pyromark sample, it has more dense surface structure that can make micro-cracks in as-prepared state as shown in **Fig. 28**(a)-Pyromark. This micro-crack will be the driving force for delamination after a long time use at high temperature.

CuFeMnO4 (PT) / CuCr2O4 (DB)   **Co3O4 (PT) / Co4O4 (DB)**   **Pyromark**
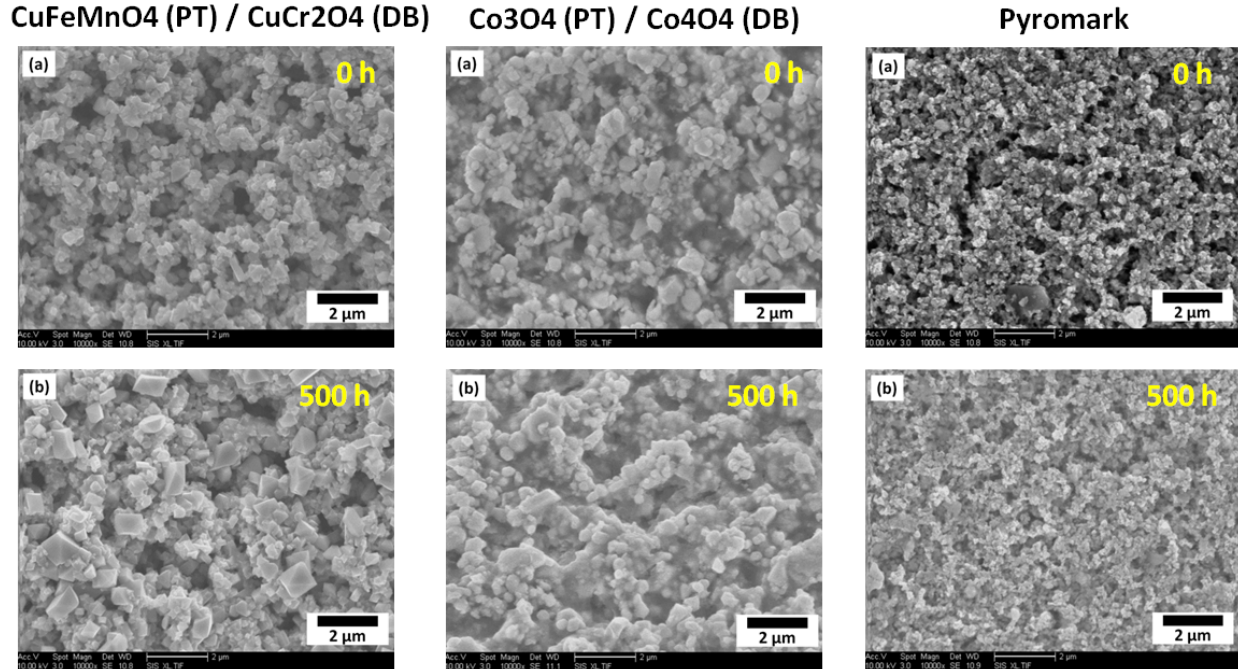
Fig. 28. SEM images showing surface morphologies of as-prepared samples (0h) and samples annealed at 750°C/500h/air, and observed in tilted angle of 30 degree.

Fig. 29 implies that all samples do not have severe delamination problem of their coating layers, after this harsh isothermal test (750°C/500h/air). The surface color can be different from real colors because of different light environment during photographing.
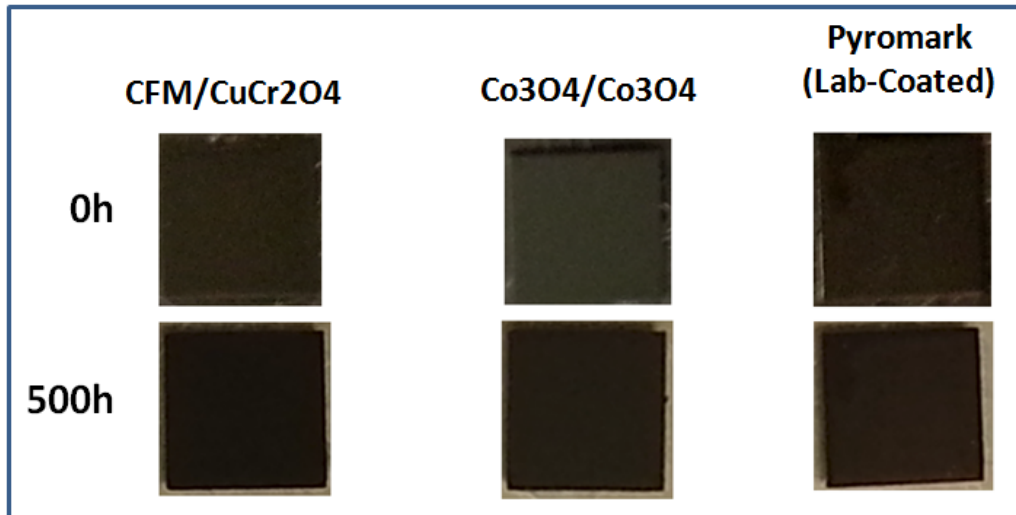
Fig. 29. Photos of samples taken before (0h) and after isothermal test (750°C/500h/air).

Table 13 is a summary of all FOM endurance evaluation data from which it can be found out that isothermal annealing gives more detrimental effect on the optical property because a long time isothermal test decreased FOM values more than thermal cycling test. For instance, CuFeMnO4/CuCr2O4 sample satisfies both FOM endurance goal

(0.98) and high FOM goal (0.90), **CuFeMnO4/CuCr2O4 sample decreases FOM endurance with thermal test conditions; 0.9989 (after thermal cycling) → 0.9978 (after isothermal annealing at 600°C) → 0.9922 (after isothermal annealing at 750°C)**. In future research, it is necessary to fabricate nanoparticles with better size stability at high temperature and to develop new doped particles with other elements which can stabilize particle's size and structure more at high temperature in air.

Table 13. Summary of FOM endurance evaluation results.

		600C/ 1000h	600C/ 100cycles	750C/ 500h	750C/ 100cycles
CuFeMnO4(PT)/ CuCr2O4(DB)	As-prepared (0h, or 1cycle)	0.901	0.899	0.903	0.902
	After thermal test (mean)	**0.899**	**0.898**	**0.896**	**0.901**
	FOM Endurance	**0.9978**	**0.9989**	**0.9922**	**0.9989**
Co3O4(PT)/ Co3O4(DB)	As-prepared (0h, or 1cycle)	0.865	0.864	0.865	0.866
	After thermal test (mean)	**0.863**	**0.860**	**0.859**	**0.865**
	FOM Endurance	**0.9977**	**0.9954**	**0.9931**	**0.9988**
Pyromark (DS) (Lab-Coated)	As-prepared (0h, or 1cycle)	0.895	0.895	0.898	0.897
	After thermal test (mean)	**0.893**	**0.892**	**0.893**	**0.895**
	FOM Endurance	**0.9978**	**0.9966**	**0.9944**	**0.9978**
Pyromark (CSP Company)	As-prepared (0h, or 1cycle)	-	-	-	0.871
	After thermal test (mean)	-	-	-	**0.858**
	FOM Endurance	-	-	-	**0.9851**

4.2 Repairability of CFM(PT)/CuCr2O4(DB) Samples

An impaired sample of CuFeMnO4/CuCr2O4 was made intentionally by scratching the surface, as shown in a left photo of Fig. 30. And new spray-coating was carried out to make coating of CuCr2O4 dense layer followed by another coating of porous

CuFeMnO4 layer as shown in the second photo of Figure 12. After the isothermal annealing (600°C/1000h/air), there is no delamination problem as shown in a right photo of Figure 12.
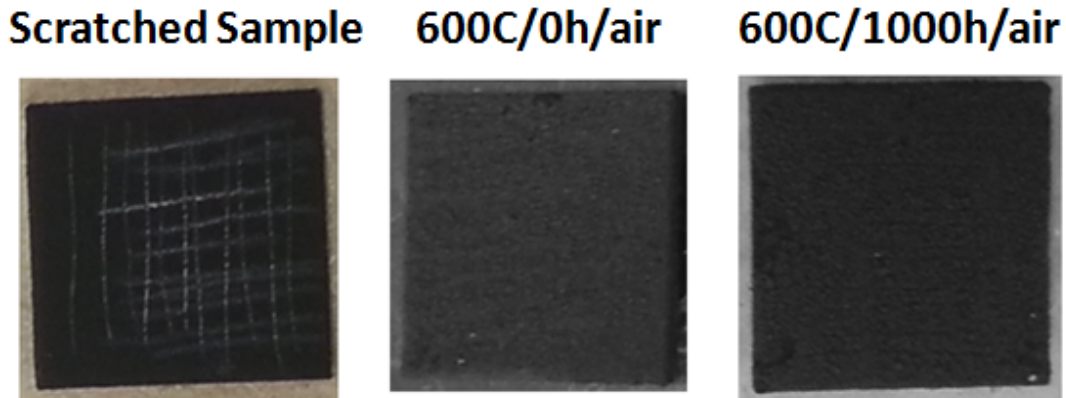
Fig. 30. Photos for (left) an impaired CuFeMnO4/CuCr2O4 sample by scratching, (middle) a repaired sample by new spray coating on the scratched surface, and (right) a repaired sample after isothermal test.

Fig. 31 shows the repaired CuFeMnO4/CuCr2O4 sample recovers to achieve high FOM value (0.899) and the FOM value still keeps 0.90 after isothermal test (600°C/1000h/air). In Figure 31, the reflectance decreases slightly in visible spectrum and increases near 2um, which causes the FOM to improve in a small amount.

As shown in Table 14, **the repaired CuFeMnO4/CuCr2O4 sample satisfies both FOM endurance goal (0.98) and high FOM goal (>Pyromark) after isothermal annealing at 600°C**.
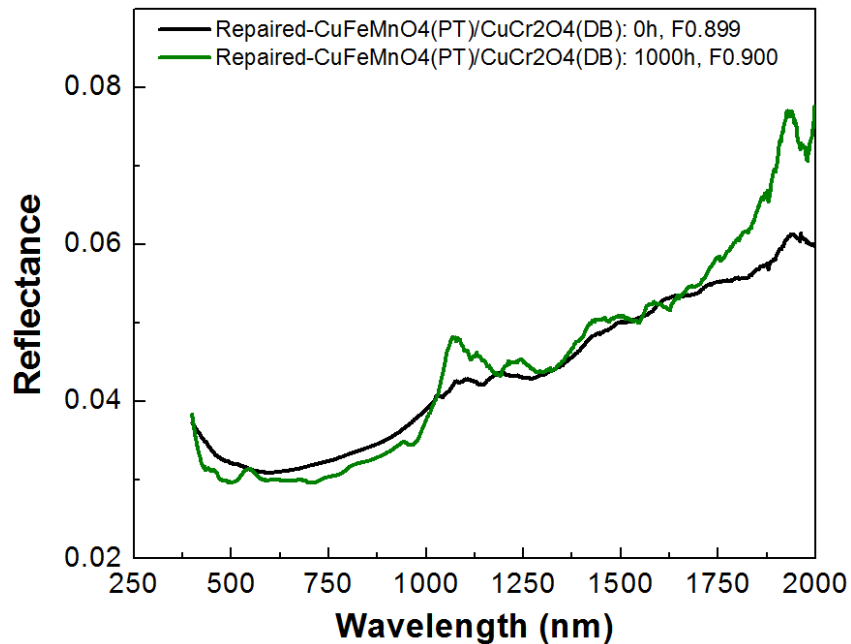
Fig. 31. Reflectance and FOM comparison between as-repaired CuFeMnO4/CuCr2O4 (0h) and annealed one (600°C/1000h/air).

Table 14. FOM endurance of repaired CuFeMnO4/CuCr2O4 sample after isothermal annealing at 600°C/1000h/air, based on mean values and minimum values in 95% confidence.

0h	1000h (mean)	1000h(min. 95% Conf.)	Endurance (mean)	Endurance (min.)
0.899	**0.899**	0.898	**1.0**	**0.9989**

Table 15. t-test of FOM values obtained from reflectance measurements of CuFeMnO4/CuCr2O4 sample after isothermal annealing (600°C/1000h/air).

t-test	CFM/CuCr2O4 (Repaired)
1	0.8986
2	0.8986
3	0.8985
4	0.9000
5	0.8992
Mean Value	**0.89898**
Std Deviation	0.00063403
95% Conf. Min.	**0.89819287**

4.3 Adhesion of CFM(PT)/CuCr2O4 (DB) samples

The milestone regarding the adhesion is to maintain a retained area greater than 95% after thermal tests. Fig. 32 shows that the **CFM(PT)/CuCr2O4(DB) sample has excellent adhesion (all greater than 98.7) after all the four different types of thermal tests, thereby satisfying the adhesion milestone (95%)**.

Furthermore, Fig. 33 shows that the **repaired CFM(PT)/CuCr2O4(DB) sample has a good adhesion (98.3%) as well after isothermal test (600°C/1000h/air), which is much better than the required milestone (95%).**

**Thermal Cycle
(RT-600C/100cycles/air)**

%Area
98.705

**Isothermal
(600C/1000h/air)**

%Area
98.889

**Thermal Cycle
(RT-750C/100cycles/air)**

%Area
99.023

**Isothermal
(750C/500h/air)**

%Area
98.781
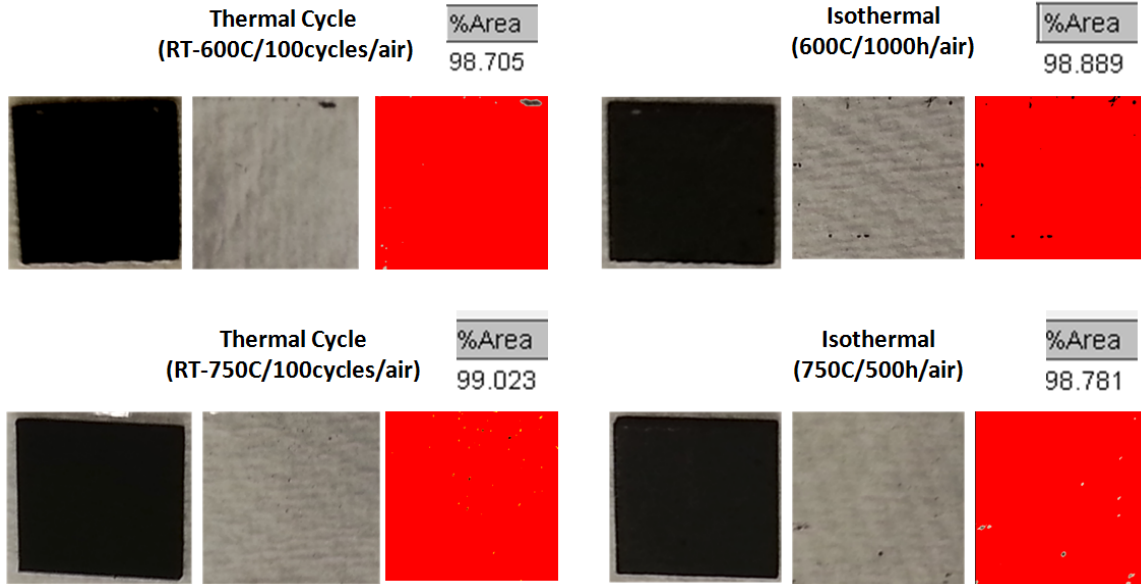
Fig. 32. Adhesion evaluation for CFM(PT)/CuCr2O4(DB) sample after thermal tests. In each thermal test, The left is the sample image after removing tapes, the middle is the image of the detached tape, and the right is ImageJ-processed image which yields the retained area percentage.

Before Isothermal Test

%Area
98.420

After Isothermal Test

%Area
98.296
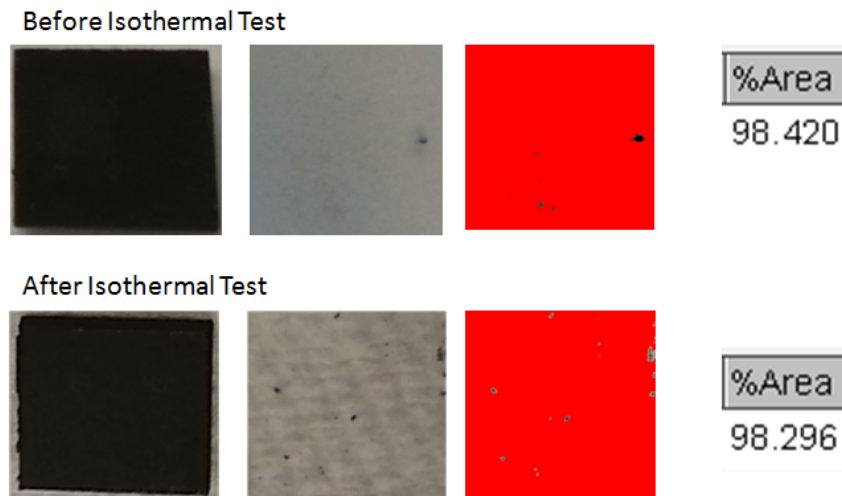
Fig. 33. Adhesion evaluations for **repaired** CuFeMnO4/CuCr2O4 in the as-prepared state and after isothermal test (600°C/1000h/air). In each thermal test, The left is the sample image after removing tapes, the middle is the image of the detached tape, and the right is ImageJ-processed image which yields the retained area percentage.

Table 16. t-test of retained area percentage by tape test in CFM(PT)/CuCr2O4(DB) sample and its repaired sample.

t-test	600C/ 1000h	600C/ 100cycles	750C/ 500h	750C/ 100cycles	600C/ 1000h (repaired)
1	98.9	98.7	98.8	99.0	98.3
2	98.9	98.8	98.7	99.0	98.2
3	98.7	98.7	98.8	98.9	98.5
4	98.9	98.6	98.8	99.0	98.3
5	98.7	98.7	98.8	99.0	98.3
AVR	98.82	98.7	98.78	98.98	98.32
Standard Dev	0.109544512	0.070710678	0.04472136	0.04472136	0.109544512
Min. w/ 95% Confidence	98.68400433	98.61221517	98.72448	98.92448	98.18400433

5   Summary of the Achieved Milestones

Mile-stone	Metric (From Measurement)	Success Value	Measured Value	Assessment Tool	Conclusion
3.1.1	SSC Adhesion [t = 1000h; 600C] $\frac{(\text{Total Test Area} - \text{Area Lost})}{\text{Total Test Area}}$	>0.95 and greater than Pyromark	CFM/CuCr 0.989 0.989 0.987 0.989 0.987		Success
3.1.2	Isothermal Endurance of FOM Success Value defined as: $\frac{FOM[t = 1000h; 600C]}{FOM[t = 0; 600C]}$	0.98 and greater than Pyromark	CFM/CuCr 0.9966 0.9973 0.9974 0.9977 0.9974	Co3O4 0.9965 0.9963 0.9980 0.9972 0.9978	Success
3.1.3	SSC Adhesion [n = 100; 25C to 600C] $\frac{(\text{Total Test Area} - \text{Area Lost})}{\text{Total Test Area}}$	>0.95 and greater than Pyromark	CFM/CuCr 0.987 0.988 0.987 0.986 0.987		Success
3.1.4	Thermal Cycling Endurance of FOM Success Value defined as: $\frac{FOM[n = 100; 25 \text{ to } 600C]}{FOM[n = 1; 25 \text{ to } 600C]}$	0.98 and greater than Pyromark	CFM/CuCr 0.9981 0.9990 0.9996 1.0004 0.9993	Co3O4 0.9951 0.9950 0.9951 0.9956 0.9954	Success
3.2.1	Establish contacts with at least one CSP companies and have at least one discussion meeting		By the end of Q1		Completed
3.2.2	Formulate the strategies and specs sheet together with the commercial partner(s) on optimizing the SSC coating materials		By the end of Q2		Completed
3.2.3	Discuss/determine with the commercial partner(s) on how to best pursue commercial applications.		By the end of Q4		Completed
3.3.1	SSC Adhesion of **Repaired SSC** [t = 0h; 600C] $\frac{(\text{Total Test Area} - \text{Area Lost})}{\text{Total Test Area}}$	>0.95 and comparable or greater than Pyromark	CFM/CuCr 0.985 0.987 0.984 0.991 0.983		Success
3.3.2	FOM of **Repaired SSC**	98% ×0.90 and comparable greater than Pyromark	Repaired CFM/CuCr 0.899 0.899 0.899 0.900 0.899		Success vs. Pyromark: F 0.896
3.3.3	SSC Adhesion of **Repaired SSC** [t = 100h; 600C] $\frac{(\text{Total Test Area} - \text{Area Lost})}{\text{Total Test Area}}$	>0.95 and comparable or greater than Pyromark	CFM/CuCr 0.983 0.982 0.985 0.983 0.983		Success
3.3.4	Isothermal Endurance for **Repaired SSC** Success Value defined as: $\frac{FOM[t = 1000h; 600C]}{FOM[t = 0; 600C]}$	0.98 and comparable or greater than Pyromark	CFM/CuCr 0.9996 0.9996 0.9994 1.0011 1.0002		Success

			CFM/CuCr	Co3O4	
3.4.1	SSC Adhesion [t = 500h; 750C] $$\frac{(Total\ Test\ Area - Area\ Lost)}{Total\ Test\ Area}$$	>0.95	0.988 0.987 0.988 0.988 0.988		Success
3.4.2	Isothermal Endurance of FOM Success Value defined as: $$\frac{FOM[t = 500h; 750C]}{FOM[t = 0; 750C]}$$	0.98	0.9918 0.9917 0.9916 0.9927 0.9917	0.9923 0.9929 0.9933 0.9926 0.9924	Success
3.4.3	SSC Adhesion [n = 100; 25C to 750C] $$\frac{(Total\ Test\ Area - Area\ Lost)}{Total\ Test\ Area}$$	>0.95	0.990 0.990 0.989 0.990 0.990		Success
3.4.4	Thermal Cycling Endurance of FOM Success Value defined as: $$\frac{FOM[n = 100; 25\ to\ 750C]}{FOM[n = 1; 25\ to\ 750C]}$$	0.98	0.9993 0.9994 0.9990 0.9987 0.9990	0.9995 1.0007 0.9990 0.9998 0.9990	Success

-

6 Conclusion and Outlook

In conclusion, **we have successfully developed solar absorbing coatings that simultaneously meet all the stringent requirements** for next generation high-temperature CSP systems. Specifically, through a systematical investigation we have identified the optimal composition of Cu Ion Manganese Oxide and Cu Chromite, namely $Cu_1Fe_1Mn_1O4$ (CFM) and $CuCr_2O_4$. We have also developed novel and scalable process to create porous structures upon spray coating using sacrificial polymer beads. Furthermore, we have utilized a tandem two-layer structures consisting of a porous top (PT) CFM layer and a dense bottom (DB) $CuCr_2O_4$ layer. This particular structure leads to **the record-high FOM value of 0.902** (assuming 1000-sun and 750°C receiver temperature), which is higher than that of the commercial paint (Pyromark). The same CFM(PT)/CuCr2O4(DB) coating also **meets all the FOM endurance and adhesion** requirements (>98% and >95% respectively) after all the thermal tests, including thermal cycling from RT to 600°C for 100 cycles and RT to 750°C for 100 cycles, as well as isothermal annealing at 600°C for 1000 hours and 750°C for 500 hours, all done in air.

We also demonstrated that a damaged (by scratching) coating sample can be repaired by simply spray coating a new CFM(PT)/CuCr2O4(DB) layer directly onto the damaged sample. The repaired sample showed excellent adhesion and thermal durability as the freshly prepared samples. This result shows the on-site repairability of our newly developed solar coating material and process.

It is remarkable that our new coating material is outperforming that of Pyromark that is currently used in today's CSP power plants but it widely believed to be unsuitable for future high temperature CSP systems. It is envisioned that our new coating material will be a strong candidate for the next general CSP systems. To fully exploit the benefits of

our material and to bring it from the laboratory to the market, it will be necessary to perform accelerated thermal aging tests under conditions that are equivalent to 30 years and 10,000 cycles of operation at the targeted operation temperature (750°C and above). To achieve this target, suitable lifetime prediction models need to be developed and validated. Mitigation strategies to slow down the degradations need to be established. Additionally, it is also desirable to further increase the FOM beyond the current 0.90 level, for instance, by further increasing the light absorption in the solar spectrum and reducing the infrared emission. This will lead to both a lower LCOE of the CSP (due to higher efficiencies) and a longer service life of the coating.

7   Publications and Patents

Over the course of this project, the following **archival journal papers** were published, in which the Sunshot grant is acknowledged:

- J. Moon, T.K.Kim, B. VanSaders, C.Choi, Z. Liu, S. Jin, and R.Chen, "Black Oxide Nanoparticles as Durable Solar Absorbing Material for High-Temperature Concentrating Solar Power System", **Solar Energy Materials and Solar Cells**, 134, 417-424 (2015)

- T.K. Kim, B. VanSaders, J. Moon, T. Kim, c-H Liu, J. Khamwannah, R. Chen, Z. Liu, and S. Jin, "Tandem Structured Spectrally Selective Coating Layer of Copper Oxide Nanowires Combined with Cobalt Oxide Nanoparticles**", Nano Energy**, 11, 274-259, (2015)

- T.K. Kim, J. Moon, B. VanSaders, D. Chun, C.J. Gardner, J.Y. Jung, G. Wang, **R. Chen**, Z. Liu, Y. Qiao, S. Jin, "Si Boride-Coated Si Nanoparticles with Improved Thermal Oxidation Resistance", **Nano Energy** 9, 32-40 (2014)

- J. Moon, D. Lu, S.D. Kong, S. Jin, **R. Chen[#]**, Z. Liu[#], "Nanoscale Fractal Structured Spectrally Selective Coating for Solar Thermal Applications", **Nano Energy** 8, 238–246 (2014)

Additionally, one more manuscript is currently under preparation, which is focused on the development of high-FOM coating consisting of a porous top CFM layer and a dense bottom $CuCr_2O_4$ layer. Thermal stability of the same coating will also be reported.

The following patents were filed:

- S. Jin, R. Chen, Z. Liu, T.K. Kim, "Spectrally selective coatings for optical surfaces", Pub. No.: WO/2013/166521, Published Nov. 2013.
- S. Jin, R. Chen, Z. Liu, T.K. Kim, " Solar Energy Absorbing Coatings and Method of fabrication", PCT Application No.: PCT/US2015/020589, Filed March 13, 2015.

8 References

1. Cernik, R.J., et al., *Direct correlation between ferrite microstructure and electrical resistivity.* Journal of Applied Physics, 2007. **101**(10).

2. Strehlow, W.H. and E.L. Cook, *Compilation of Energy Band Gaps in Elemental and Binary Compound Semiconductors and Insulators* J. Phys. Chem. Ref. Data, 1973. **2**: p. 163.

3. Wang, G.X., et al., *Hydrothermal Synthesis and Optical, Magnetic, and Supercapacitance Properties of Nanoporous Cobalt Oxide Nanorods.* Journal of Physical Chemistry C, 2009. **113**(11): p. 4357-4361.

4. Dias, A. and V.T.L. Buono, *Hydrothermal synthesis and sintering of nickel and manganese-zinc ferrites.* Journal of Materials Research, 1997. **12**(12): p. 3278-3285.

5. Jiang, X.C., T. Herricks, and Y.N. Xia, *CuO nanowires can be synthesized by heating copper substrates in air.* Nano Letters, 2002. **2**(12): p. 1333-1338.

6. Atabaev, T.S., et al., *Facile synthesis of bifunctional silica-coated core-shell Y2O3:Eu3+,Co2+ composite particles for biomedical applications.* Rsc Advances, 2012. **2**(25): p. 9495-9501.

7. ASTM, *Standard Test Methods for Measuring Adhesion by Tape Test.* ASTM.

8. Ho, C.K., et al., *Characterization of Pyromark 2500 Paint for High-Temperature Solar Receivers.* Journal of Solar Energy Engineering-Transactions of the Asme, 2014. **136**(1).

9. Martens, J.W.D., W.L. Peeters, and M. Erman, *An Ellipsometric and Magneto-Optical Study of Cobalt Ferrite Single-Crystals.* Solid State Communications, 1982. **41**(9): p. 667-669.

10. Simsa, Z., et al., *Optical and Magneto-Optical Properties of Magnetite and Manganese Ferrites.* Journal of Magnetism and Magnetic Materials, 1980. **15-8**(Jan-): p. 775-776.

11. Simsa, Z., et al., *Optical-Properties of Manganese Ferrites.* Physica Status Solidi B-Basic Research, 1979. **96**(1): p. 137-144.

12. Karlsson, B. and C.G. Ribbing, *Optical-Constants and Spectral Selectivity of Stainless-Steel and Its Oxides.* Journal of Applied Physics, 1982. **53**(9): p. 6340-6346.